Loss-of-function of RNA-binding protein PRRC2B causes translational defects and congenital cardiovascular malformation

Debojyoti Das[1,#], Eng-Soon Khor[1,#], Feng Jiang[1,2,#], Jiali He[1], Yui Kawakami[1], Lindsey Wainwright[1,2], Jared Hollinger[1], Joshua Geiger[3], Huan Liu[1], Fanju Meng[4], George A. Porter, Jr.[5], Zhenggen Jin[1], Patrick Murphy[4], Peng Yao[1,2,6,7*]

[1] Aab Cardiovascular Research Institute, Department of Medicine, University of Rochester School of Medicine & Dentistry, Rochester, NY 14642

[2] Department of Biochemistry & Biophysics, University of Rochester School of Medicine & Dentistry, Rochester, New York 14642

[3] Department of Vascular Surgery, University of Rochester School of Medicine & Dentistry, Rochester, New York 14642

[4] Department of Biomedical Genetics, University of Rochester School of Medicine & Dentistry, Rochester, New York 14642

[5] Department of Pediatrics, Medicine, and Pharmacology and Physiology, University of Rochester School of Medicine & Dentistry, Rochester, New York 14642

[6] The Center for RNA Biology, University of Rochester School of Medicine & Dentistry, Rochester, New York 14642

[7] The Center for Biomedical Informatics, University of Rochester School of Medicine & Dentistry, Rochester, New York 14642

[#] co-first author

Correspondence to Peng Yao, Ph.D., Aab Cardiovascular Research Institute, Department of Medicine, University of Rochester School of Medicine & Dentistry, Rochester, New York 14642.

E-mail: peng_yao@urmc.rochester.edu

Keywords: congenital heart disease, translation, PRRC2B, RNA-binding protein, human mutation

Abstract

Alternative splicing generates variant forms of proteins for a given gene and accounts for functional redundancy or diversification. A novel RNA-binding protein, Pro-rich Coiled-coil Containing Protein 2B (PRRC2B), has been reported by multiple laboratories to mediate uORF-dependent and independent regulation of translation initiation required for cell cycle progression and proliferation. We identified two alternative spliced isoforms in human and mouse hearts and HEK293T cells, full-length (FL) and exon 16-excluded isoform ΔE16. A congenital heart disease-associated human mutation-mimicry knock-in of the equivalent variant in the mouse genome leads to the depletion of the full-length *Prrc2b* mRNA but not the alternative spliced truncated form ΔE16, does not cause any apparent structural or functional disorders. In contrast, global genetic inactivation of the PRRC2B gene in the mouse genome, nullifying both mRNA isoforms, caused patent ductus arteriosus (PDA) and neonatal lethality in mice. Bulk and single nucleus transcriptome profiling analyses of embryonic mouse hearts demonstrated a significant overall downregulation of multiple smooth muscle-specific genes in *Prrc2b* mutant mice resulting from reduced smooth muscle cell number. Integrated analysis of proteomic changes in *Prrc2b* null mouse embryonic hearts and polysome-seq and RNA-seq multi-omics analysis in human HEK293T cells uncover conserved PRRC2B-regulated target mRNAs that encode essential factors required for cardiac and vascular development. Our findings reveal the connection between alternative splicing regulation of PRRC2B, PRRC2B-mediated translational control, and congenital cardiovascular development and disorder. This study may shed light on the significance of PRRC2B in human cardiovascular disease diagnosis and treatment.

Discovery bullet points:

1. PRRC2B has two alternative splicing isoforms, full-length and exon 16-skipped (ΔE16) mRNAs in humans and mice.
2. Full-length *Prrc2b* KO mice show no apparent cardiac phenotypes, while double KO of full-length and ΔE16 causes patent ductus arteriosus and neonatal lethality in mice.
3. Multi-omics analyses of *Prrc2b* double KO mice suggest changes in SMC cell abundance and dysregulation of translation of specific proteins in E18.5 embryos.
4. CRISPR-Cas9-mediated KO of *PRRC2B* in human cells reduces the translation of heart and valve development-related mRNAs.

Introduction

Transcriptional regulation of gene expression controls cell differentiation, tissue patterning, and organ formation. Messenger RNA (mRNA) metabolic processes after transcription also play essential roles in maintaining the accuracy of developmental programs and organismal health (1). Posttranscriptional regulation modifies the coding capacity of mRNA and modulates the translation activity for protein synthesis. A key RNA processing pathway, alternative splicing of precursor mRNA, produces multiple isoforms of mature mRNAs that often encode distinct protein isoforms (2). These protein isoforms can conduct redundant or diversified functions in cells, depending on the structural and functional relationship. In addition, translation regulatory factors modulate the rate of translation initiation or elongation, thereby precisely controlling the amount of protein products (3). It remains largely unknown how alternative splicing of translation regulatory factors impacts cell function and organ development.

Pro-rich Coiled-coil Containing Protein 2B (PRRC2B) is one of the members of the PRRC2 proteins family, which is recognized for its RNA-binding activities (4-6). A previous study suggests the involvement of PRRC2B in forming a complex with eIF4G2, a translation initiation factor that drives translation during mouse embryonic stem cell differentiation (7). Our recent findings demonstrate PRRC2B-eIF4G2 complex-mediated translational activation of a cohort of mRNAs encoding cell cycle progression-related proteins via direct physical binding of specific RNA motifs (8). However, its biological function is still largely unknown. A previous study in the animal model showed that *Prrc2b* mRNA is highly expressed in rat whole brain tissues through early embryonic to neonatal stages but lowly expressed in adulthood (9). Most recently, an endothelial cell-specific conditional knockout of *Prrc2b* gene in mice enhanced hypoxia-induced vascular remodeling and cerebral blood flow rearrangement, thereby reducing hypoxia-driven cognitive decline (10). However, it remains unclear whether PRRC2B is biologically vital for heart development.

Congenital heart diseases (CHD) are a group of abnormalities in the heart that develop at the embryonic stage. CHD, affecting ~1% of live births, is the leading cause of mortality from congenital disabilities. CHD includes various developmental defects affecting the structure of the heart or blood vessels, e.g., cardiac vessel development (11,12), resulting in impaired cardiac functions (13). CHD can be caused by rare de novo genetic mutations (often considered loss-of-function (LOF)) in genes related to normal cardiovascular development, suggesting the essentiality of genes for heart or vessel development. A more comprehensive human clinical study reported for the first time that *de novo* mutations have significantly contributed to CHD (12). Interestingly, *PRRC2B* is one of the 12 risk genes not previously identified in CHD (12). PRRC2B

has two heterozygous mutations in CHD patients, including a nonsense mutation p.R1113X and an intronic mutation (c.6381+4dupA). These two mutations are associated with mitral regurgitation and stenosis and pulmonary vein atresia and stenosis, respectively. However, the causal genotype-phenotype relationship has not been established yet.

While previous reports in human studies lead us to speculate that PRRC2B might be associated with CHD, no reports are available for its biological role in the heart *in vivo*. This study discovered two alternative spliced isoforms of *PRRC2B* mRNA in humans and mice. We performed a bioinformatic analysis of PRRC2B associated with cardiac genetic mutations in a CHD patient cohort. We then used two genetic knockout mouse models (*Prrc2b*^{KI} and *Prrc2b*^{tm1b}) to investigate the role of PRRC2B in the heart from embryonic stages through adulthood. Our data suggest that loss of both isoforms of PRRC2B causes a deficiency of ductus arteriosus closure right after birth, and that the full-length isoform is not required for normal embryonic cardiac development and healthy status at the early postnatal stage. Our work reveals that the alternative splicing of PRRC2B provides a truncated isoform that can guard organisms against the loss of function of the full-length protein to maintain cardiovascular integrity and organismal well-being.

Results

Alternative splicing generates two conserved mRNA isoforms of PRRC2B in humans and mice

Recent reports from our and other laboratories have demonstrated the translation-regulatory function of PRRC2B in human cells (8,14). *PRRC2B* is highly expressed in the aorta and coronary artery in the cardiovascular system in humans **(Figure S1A)**. Whereas *Prrc2b* mRNA expression is expressed in murine hearts as early as E12.5 and becomes moderately reduced after birth with time into adulthood **(Figure S1B)**. We searched the NCBI and GTEx Portal databases and identified two alternative splicing (AS) mRNA isoforms for PRRC2B, full-length (FL; 32 exons in humans and 31 exons in mice) and exon 16-excluded (ΔE16; with no exon 16), which are evolutionarily conserved in humans and mice (**Figure 1A**). The exon 16 (2082-bp) encodes amino acids 775-1468 that contain RNA-binding Arg-Gly (RG) repeat motifs for interacting with target mRNAs for humans (8), implying a potentially reduced RNA-binding and translation activity of ΔE16 compared to the full-length protein. Our prior findings show that the 750-1500 aa of PRRC2B protein can primarily mediate the interaction with target mRNAs (8). These two alternative spliced isoforms were annotated across various human organs in the GTEx Portal database (**Figure S1C**). The mouse *Prrc2b* exon 16 (2253-bp) encodes amino acids 809-1558 that bear the conserved RNA-binding RG repeat motifs as in humans. RNA-seq of mouse heart tissues demonstrated the existence of exon-exon junction reads across exons 15 and 16, exons 16 and 17, and exons 15 and 17 (**Figure 1B**), confirming the AS event *in vivo*. Our RT-PCR data also validated the presence of the two AS mRNA isoforms in human AC16 ventricular cardiomyocyte cells and HEK293T cells (**Figure 1C**), immortalized human cardiac fibroblast (IHCF), as well as mouse hearts (**Figure S1D, E**). The protein structure has been predicted by Alpha-Fold (15,16) for human FL PRRC2B and mouse and human ΔE16 PRRC2B, but not for mouse FL proteins **(Figure 1D)**. Most of the regions of both protein isoforms are predicted to form intrinsically disordered regions (IDRs), including the exon 16-encoded region. Convincingly, we found the direct proteomic evidence to support the existence of human ΔE16 as a peptide spanning exon 15 and 17 was identified (SSDTLAMDMRVRSPDEALPGGLSGCSSGSGHSPYALE; red for exon 15 and green for exon 17 sequences) in the database of ProteomicsDB.

Genetic variants of PRRC2B are associated with congenital heart defects in humans

Recent reports suggest that two human PRRC2B de novo mutations are related to CHD with vascular defects in mitral valves or pulmonary veins (12,17). To further validate this genetic correlation, we performed gene-based burden testing of rare variants within the PRRC2B gene

of 3,740 CHD probands in the genetic mutation databases from the Pediatric Cardiac Genetics Consortium (PCGC) (18). The test variants have minor allele frequency (MAF) less than 0.1% in the gnomAD database and combined annotation-dependent depletion score (CADD) higher than 20, indicating strong deleteriousness of single nucleotide variants in the human genome. The outcome revealed enrichment in probands with atrial septal defects (**Table S1**; $P < 0.0001$). Hypoplastic left heart syndrome (HLHS) showed a trend toward enriching rare variants of *PRRC2B* ($P = 0.02508$). However, this phenotype did not reach significance when correcting for multiple testing.

PRRC2B contains numerous arginine (Arg) amino acid residue sites. This amino acid is often found in RNA binding regions due to its positive charge at physiologic pH (19). Signals that indirectly assess for changes in the RNA binding capacity of PRRC2B have been tested, given the hypothesis that structural alterations in RNA binding domains within the gene may contribute to congenital heart disease phenotypes. Given this, rare variants at Arg sites throughout PRRC2B were assessed for enrichment in CHD phenotypes. Again, there is an enrichment in rare damaging variants within arginine sites in *PRRC2B* in probands with atrial septal defects compared to all other probands. Interestingly, one proband was identified with a heterozygous *de novo* Arg-to-stop codon mutation p.R1113X in our analysis of the PCGC database (18). This proband had mitral regurgitation and mitral stenosis and has been previously reported as a CHD-associated gene (12). Taken together, these findings reveal a significant association of genetic variants of PRRC2B with congenital heart defects in humans, indicating a potential role of PRRC2B in heart development.

Homozygous human mutation mimicry p.R1128X knock-in mice do not manifest cardiac functional defects

The R1113X premature termination codon resides in exon 16 of the human *PRRC2B* gene. This Arg residue is highly conserved across multiple vertebrate species (Figure S2A). In mice, R1128 is the equivalent amino acid residue of R1113 in humans. Theoretically, the genetic mutation of R1113X in humans is supposed to cause nonsense-mediated mRNA decay to the full-length *Prrc2b* mRNA containing exon 16 but not the alternatively spliced truncated isoform without exon 16. To investigate whether the human heterozygous p.R1113X mutation contributes to any potential congenital heart defects *in vivo*, we generated a *Prrc2b* global knock-in (KI) mouse model using the CRISPR (clustered regularly interspaced short palindromic repeats) technology. The global KI mice were created by introducing an Arg-to-stop codon at the position of 1128 amino acid (p.R1128X) and two additional wobble base mutations (GACTTC-to-GATTTT) using a guide

RNA and a homology-directed recombination DNA template (**Figure 2A**). TA cloning and DNA Sanger sequencing confirmed the successful replacement of a premature stop codon at the Arg codon into the *Prrc2b* genomic locus (**Figure 2B**). Both heterozygous and homozygous *Prrc2b* KI mice are viable and fertile, and their offspring follow the Mendelian ratio.

We reasoned that potential ΔE16 isoform expression might compensate for the loss of full-length (FL) PRRC2B protein isoform to maintain the viability of the KI mice. As expected, the FL *Prrc2b* mRNA expression was reduced drastically by nonsense-mediated mRNA decay in the heart of *Prrc2b* p.R1128X KI (FL-*Prrc2b*^{gKO}) mice, based on quantitative measurements of *Prrc2b* expression using RT-qPCR for heart tissue lysates (**Figure S2B**) (primers #1, #3, and #4). In contrast, the ΔE16 *Prrc2b* mRNA isoform expression was unaffected (primers #2, #5, and #6). To examine whether KO of FL *Prrc2b* mRNA expression causes any cardiac functional changes, echocardiography was performed to measure the left ventricular function. We observed no significant changes in LV mass in the KI mice up to 3 months after birth (**Figure 2C; Table S2**). When comparing WT and KI mice, ejection fraction, fractional shortening, or cardiac output did not change from 1 to 3 months post-birth (**Figure 2D-F; Table S2**). After 5 months, we did not observe a significant difference in heart size or collagen deposition in KI mice compared to WT mice (**Figure 2G, H**). H&E imaging analysis did not uncover any apparent structural difference in multiple organs of KI versus WT mice, including brain, kidney, liver, lung, skeletal muscle (**Figure S2C**), spleen, and thymus (data not shown). These results suggest that loss of the full-length PRRC2B in mice does not cause any significant cardiac pathological phenotypes, e.g., cardiac hypertrophy or fibrosis and left ventricular functional decline, in adulthood at the baseline.

Homozygous *Prrc2b*^{tm1b} mice exhibit patent ductus arteriosus and neonatal lethality

Our phenotyping data of *Prrc2b* p.R1128X KI (FL-*Prrc2b*^{gKO}) mice suggested that loss of the FL PRRC2B isoform does not significantly affect cardiac structure or function (**Figure 2**). This may indicate the ΔE16 PRRC2B protein can compensate for the loss of the full-length protein. Therefore, we were tempted to produce a mouse model with both alternative spliced *Prrc2b* isoforms nullified, termed *Prrc2b*$^{tm1b-/-}$. The tm1b-LacZ tagged null allele was generated by deletion of the critical fourth exon of the *Prrc2b* genomic locus and the neomycin cassette using a constitutive CMV-Cre recombinase that recognizes loxP sites **(Figure 3A)**. This allele is considered an authentic knockout, as skipping over the LacZ cassette cannot restore *Prrc2b* expression.

The elimination of the fourth exon at the genomic level was validated by DNA genotyping **(Figure S3A)**. In addition, the absence of both FL and ΔE16 *Prrc2b* mRNA transcripts in *Prrc2b*$^{tm1b-/-}$ mice

was confirmed by RNA-seq and agarose gel electrophoresis following real-time PCR **(Figure 3B, C, S2A, S3B, C)**. This suggests that phenotypes observed in *Prrc2b*$^{tm1b-/-}$ mice represent the consequence of the loss-of-function of both *Prrc2b* AS isoforms. We observed preweaning lethality of homozygous *Prrc2b*$^{tm1b-/-}$ mice in 18 litters from the heterozygote breeding **(Figure 3D, left)**. Thus, we assumed that *Prrc2b*$^{tm1b-/-}$ pups might have died *in utero* or perinatally after a normal vaginal delivery. Indeed, we have obtained 24 alive *Prrc2b*$^{tm1b-/-}$ pups in 11 litters ranging from different prenatal stages (E12.5, E13.5, E14.5, E17.5, and E18.5) to the early postnatal stage (P0) **(Figure 3D, right)**. This suggests that *Prrc2b*$^{tm1b-/-}$ mice are alive at the prenatal stage. Subsequently, we successfully captured the live *Prrc2b*$^{tm1b-/-}$ neonatal mice as early as 7 hours post-birth **(Figure 3E)**. The LacZ cassette was expressed in tissues where the Prrc2b gene was knocked out. β-galactosidase staining was used to examine the tissue expression of Prrc2b at different developmental stages and across multiple organs. A dark blue LacZ signal was evident in *Prrc2b*$^{tm1b-/-}$ and *Prrc2b*$^{tm1b+/-}$ but not in WT embryonic hearts isolated at E12.5 **(Figure S3D)**. The LacZ signals were also detected in the heart, brain, pituitary, aorta, olfactory bulbs, bladder, and thymus. Still, they were barely detected in the skeletal muscle and lung from the *Prrc2b*$^{tm1b+/-}$ and WT adult mice (4-month-old) **(Figure S3E)**. This suggests the active transcriptional activity of *the Prrc2b* gene promoter, ranging from prenatal to late-postnatal stages across multiple organs and cell types.

As *PRRC2B* human mutations were reported to be associated with mitral valve stenosis or pulmonary vein atresia and stenosis (12,17), we next examined the state of blood vessels in the heart. We injected Coomassie blue dye into the heart's left ventricle isolated from WT control and *Prrc2b*$^{tm1b-/-}$ mice. Interestingly, we observed that the ligamentum arteriosum (LA) has a white band with the exclusion of the blue dye in the *Prrc2b*$^{tm1b-/-}$ heart but not in the WT heart, suggesting the failure of ductus arteriosus (DA) closure at P0 **(Figure 3F)**, leading to patent ductus arteriosus (PDA). In contrast, the PDA did not occur at the earlier time point (E17.5) in the alive *Prrc2b*$^{tm1b-/-}$ prenatal mice **(Figure 3G)**. At E17.5, DA shunts away the blood from the PA to the aorta in the embryonic/fetal circulation. There is no difference in all three genotypes (WT, *Prrc2b*$^{tm1b+/-}$, and *Prrc2b*$^{tm1b-/-}$) as the blood in E17.5 mice is present throughout the DA vessel. However, at P0, the transformation of DA into LA, which marked the closure, occurred in *Prrc2b*$^{tm1b+/-}$ and *Prrc2b*^{WT}, whereas PDA was observed in *Prrc2b*$^{tm1b-/-}$ as the DA remained open. This phenotype was not seen in heterozygous or WT littermates **(Figure 3F)**. Hematoxylin and eosin (H&E) staining of the frontal section of the heart tissues of *Prrc2b*$^{tm1b+/-}$ and WT mice further confirmed the sustained opening of the PDA in the homozygous KO hearts but not in the control hearts **(Figure 3H)**. These findings suggest that *Prrc2b* loss-of-function leads to PDA in mice and, thus, neonatal lethality

within ~24 hours after birth, consistent with the general observation of sustained PDA leading to neonatal lethality (20,21). Also, comparing the phenotypes between *Prrc2b* p.R1128X KI and *Prrc2b*$^{tm1b-/-}$ mice, we indicate that the ΔE16 PRRC2B protein isoform may compensate for the loss of full-length PRRC2B function *in vivo*.

Transcriptomic profiling reveals alterations of gene expression related to translation, mitochondria, smooth muscle cell, and cardiovascular development in *Prrc2b*$^{tm1b-/-}$ mice

PRRC2B is identified as an RNA-binding protein by unbiased mRNA interactome capture analysis using mass spectrometry (4-6). Our recent findings suggest that PRRC2B can bind to specific RNA motifs and activate the translation of a selective cohort of cell proliferation-related mRNAs (8). Another laboratory shows that PRRC2B promotes the leaky scanning of uORFs, thereby enhancing the translation of main ORFs (14). To shed light on the molecular function of PRRC2B in the heart, we performed paired-end RNA-seq on whole hearts of *Prrc2b*$^{tm1b-/-}$ and WT mice at E18.5. We identified 42 upregulated and 36 downregulated genes that are significantly changed in knockout (KO) heart samples compared to WT controls ($P < 0.05$ or $P_{adj} < 0.05$) **(Figure 4A, B, S4A, B; Table S3)**. Gene ontology analysis revealed that pathways of translation and mitochondria, such as cytoplasmic translation, mitochondrial respiratory chain complex I assembly, and mitochondrial ATP synthesis coupled proton transport were among the top downregulated biological processes in KO hearts **(Figure 4C, S4C)**. Critical genes in translation machinery and mitochondria were significantly reduced at the mRNA steady-state levels, such as ribosomal protein genes (*Rps29*, *Rps28*, *Rpl37*, *Rpl39*) and essential mitochondrial genes, including *Lars2*, *Tomm7*, *Ndufb4*, *Uqcr11*, *Ndufa1*, *mt-Nd2*, *mt-Atp6*, *mt-Cytb*. In addition, multiple pathways related to cardiovascular development and blood vessel formation were among the top upregulated biological processes in KO hearts, including extracellular matrix (ECM) organization, positive regulation of cell migration, response to mechanical stimulus, negative regulation of endothelial cell migration, negative regulation of smooth muscle cell proliferation, and blood vessel remodeling **(Figure 4D, S4C)**. These genes with increased steady-state mRNA levels include *Postn, Meox1*, *Thbs1*, *Col11a1*, *Bmper*, and *Adamtsl2,* among other ECM protein-coding genes.

Among the top 20 differentially expressed genes (DEG), we noticed that *Lmod1* and *mt-Atp6* were drastically reduced ($P < 0.05$). In contrast, multiple transmembrane or secretory protein-encoding genes *Matn4*, *Ptx3*, *Slc22a1*, *Plppr5*, *Dct*, *Cpne5*, *Pmel*, *Shisa2*, and *Bmp2* were significantly increased ($P < 0.05$) **(Figure 4E)**. The RNA-seq reads of *Prrc2b* mRNA were drastically decreased in *Prrc2b* null hearts, confirming the genetic KO effect at the gene expression level.

Intriguingly, overlapping our identified DEG with the reported list of genes involved in mouse or human PDA revealed four mouse PDA genes **(Figure 4F)**, including *Myh11* and *Smarca4* reduced in *Prrc2b* KO heart samples. qPCR validation not only further confirmed the significantly reduced expression of *Myh11* and *Smarca4* mRNAs but also other SMC mRNAs, including *Acta2* and *Actg2,* and mitochondrial mRNAs such as *Nd2* and *Atp6* **(Figure 4G)**, in E18.5 KO hearts. This indicates that the vascular smooth muscle contraction essential for ductus arteriosus closure may be impaired in the *Prrc2b* knockout heart, which culminates in PDA phenotypes.

Single nucleus analysis of transcriptome in wild-type and *Prrc2b*$^{tm1b-/-}$ E18.5 hearts indicates a reduced number of smooth muscle cells

PRRC2B is an RNA-binding protein expressed in multiple organs and cell types. To further examine the cell type-specific gene expression in KO hearts, we conducted single-nucleus RNA-sequencing (snRNA-seq) to measure gene transcription changes across distinct cardiac cell types in WT and homozygous *Prrc2b*$^{tm1b-/-}$ mice (**Figure 5A**). We obtained expression profiles for 13,665 nuclei with a median of 3,433 RNA-seq reads per nucleus. These nuclei include 4,660 nuclei from WT hearts and 4,592 from *Prrc2b*$^{tm1b-/-}$ hearts.

Utilizing Seurat, we identified 22 distinct clusters, which we subsequently annotated based on the RNA expression patterns of well-established lineage-specific marker genes (**Figure 5B, C, S5A**). These 16 clusters collectively represent seven major cardiac cell types: ventricular cardiomyocytes (Ven.CM), atrial cardiomyocytes (Atri.CM), fibroblasts (FB), endothelial cells (EC), smooth muscle cells (SMC), pericytes, and epicardial cells. We observed a good quality of the data based on the number of genes (nfeature), number of reads (ncount), percentage of mitochondrial coded genes (**Figure S5B-D**), and correlation between the number of genes (nfeature, y-axis) and number of reads detected in each nucleus (**Figure S5E**). Notably, we found that cell number was significantly decreased in SMC, endocardial/lymphatic EC, epicardial cells, and endocardial cells from homozygous KO hearts compared to WT hearts (**Figure 5D**). In contrast, the abundance of CM nuclei in homozygous KO hearts increased compared to WT ones (**Figure 5D**). Subsequently, we examined the differential gene expression patterns between WT and *Prrc2b* KO hearts. Intriguingly, we did not find evidence supporting significant gene expression differences in SMC from KO hearts compared to WT hearts, suggesting a reduced SMC cell number in the KO hearts compared to the control hearts, which led to reduced SMC-related gene expression in the bulk RNA-seq analysis as shown above (**Figure 5E; Table S4**).

Quantitative mass spectrometry analysis reveals specific proteomic changes *in vivo*

We previously demonstrated that PRRC2B plays a role in the translational regulation of specific target mRNAs for protein synthesis (8). To determine if protein expression is affected in the *Prrc2b*$^{tm1b-/-}$ mice, we subjected the homozygous KO and WT control mouse hearts to mass spectrometry analysis and discovered the reduction of a specific cohort of proteins (**Figure 6A; Table S5**). Statistically, significantly downregulated proteins are enriched in five GO pathways of positive regulation of G1/S transition of the mitotic cell cycle, DNA replication, protein neddylation, mitochondrial respiratory chain complex IV assembly, and translation (**Figure 6B**). In contrast, GO analysis could not obtain any enriched pathways for upregulated proteins due to the limited number of genes. We further investigated downregulated protein with a cut-off as $Log_2FC < -0.75$. We revealed multiple highly enriched pathways, including mitochondrial translation, mitotic cytokinesis, membrane fission, glycolysis, epithelial cell migration, and cardiac muscle contraction (**Figure 6C**). These changes were discovered in the whole heart tissue and indicate a compromise of certain functional proteins for maintaining normal cardiac cell structure and function. However, we could not assign these changes to any specific cardiac cell type.

Knockdown of PRRC2B leads to abnormal cardiac morphology in zebrafish

To determine whether PRRC2B is evolutionarily crucial and conserved in normal cardiac development, we knocked down *Prrc2b* gene expression using both splicing- and translation-blocking morpholino (MO) antisense oligonucleotides in zebrafish (**Figure S6A**). RT-PCR data suggest that intron 3 (106 bp) of *Prrc2b* was retained in the mRNA, which yielded a higher band as observed in the agarose gel (**Figure S6B**). As a result, introducing three premature stop codons within this intron is likely to trigger nonsense-mediated mRNA decay and thus reduce the protein expression of PRRC2B. We have observed pericardial edema and heart looping defect present only in five *Prrc2b* morphant zebrafish (5/30; penetrance of 16.7%) injected with splicing-blocking MO but not in control zebrafish (0/25) **(Figure S6C)**. However, 86.7% of the *Prrc2b* morphant zebrafish (52/60) injected with translation-blocking MO were found dead 3 days post-injection, likely due to severe abnormalities in the heart development as a low amount of PRRC2B protein can be produced in this case. The eight-surviving fish with translation-blocking MO also showed pericardial edema, while none of the morphant zebrafish injected with control MO showed any cardiac phenotypes (0/18) (**Figure S6D**). However, since there is no suitable antibody for zebrafish PRRC2B protein, it is challenging to determine the PRRC2B protein expression level in *Prrc2b* morphant zebrafish injected with translation-blocking MO. This data suggests the importance of PRRC2B in maintaining normal cardiac development in zebrafish, which started as early as 36 hours post-fertilization (hpf) during zebrafish heart development.

Insights into conserved PRRC2B-regulated target mRNAs across cell types and species

To identify potential commonly shared PRRC2B-regulated target mRNAs in humans and mice across different organs or cell types, we created a CRISPR-derived PRRC2B KO human HEK293T cell line as confirmed by DNA Sanger sequencing and Western blotting (**Figure S7A, 7A**). In the validated PRRC2B KO HEK293T cell line, we confirmed by Sanger sequencing that three copies of PRRC2B DNA alleles were disrupted by random insertions or deletions within the exon 7 that is shared by both FL and ΔE16 PRRC2B. Therefore, both alternative spliced PRRC2B mRNA isoforms were depleted in the KO cells. Polysome profiling and puromycin incorporation assays indicated no apparent changes in global mRNA translation and *de novo* protein synthesis (**Figure 7B, S7B**). RNA-seq analysis uncovered changed gene expression at the mRNA steady-state level in *PRRC2B* KO human cells (**Figure 7C, S7C-E; Table S6**). Extracellular matrix-related genes were significantly reduced, while neurogenesis, ion channel, and cytoskeleton-related genes were increased (**Figure 7D**). The reduction of ECM genes is opposite to the increase in expression in *Prrc2b* tm1b KO hearts, suggesting ECM remodeling in the whole heart is a secondary effect of multiple cardiac cell types rather than an autonomous effect from a single cell type. In addition, PRRC2B is primarily a translation regulatory factor, and thus, the changes in mRNA steady-state levels may be an indirect consequence downstream of the translational reprogramming.

To further examine the translational reprogramming in *PRRC2B* KO human cells, we performed polysome profiling to isolate total RNA from the polysome fractions, followed by deep sequencing (polysome-seq). The polysome-seq analysis revealed PRRC2B-regulated target mRNAs when normalized to RNA-seq data to indicate the changes in translation efficiency (TE) based on the extent of enrichment of a given mRNA in actively translated polysome fractions (**Figure 7E, F, S7C-E; Table S6**). Intriguingly, among the TE-downregulated genes, many of them were highly enriched in cardiac development pathways, including aortic valve development, muscle tissue morphogenesis, semi-lunar valve development, cardiac chamber morphogenesis, endocardial cushion formation, heart morphogenesis, heart trabecula morphogenesis, and cardiac epithelial to mesenchymal transition, among others (**Figure 7G, left**). Multiple mRNAs enriched across various cardiac development pathways include *BMP2* (bone morphogenetic protein 2), *NOTCH1* (notch receptor 1), *RBPJ* (recombination signal binding protein for immunoglobulin kappa J region), *ROCK1* (Rho-associated coiled-coil containing protein kinase 1), *SNAI2* (snail family transcriptional repressor 2), *ANKRD1* (ankyrin repeat domain 1), *DSP* (desmoplakin), *MYLK* (myosin light chain kinase), *ADAMTS1* (ADAM Metallopeptidase With Thrombospondin Type 1

Motif 1), *DNAH11* (Dynein axonemal heavy chain 11), and *SOS1* (Son of sevenless homolog 1) (**Table S6**). Among these TE-downregulated proteins, the loss of function of RBPJ is known to cause PDA, and the DA-enriched enzyme ROCK1 is considered a therapeutic target for PDA (22). As a potential compensatory response, we observed mitochondrial electron transport chain and ribosome-related mRNAs were enriched in the TE-upregulated cohort (**Figure 7G, right**).

We overlapped the proteins downregulated in the *Prrc2b*$^{tm1b-/-}$ hearts with translational silenced genes in the KO HEK293T cells and inducible shRNA-mediated knockdown HEK293T cells we reported previously (8). We found 41 common hits among the three datasets, 134 shared genes between *PRRC2B* KO mouse hearts and KO human cells, and 16 additional shared genes between *PRRC2B* KO mouse hearts and knockdown human cells (**Figure 8A; Table S6**), suggesting a conserved cohort of PRRC2B-regulated mRNAs in different cell types across humans and mice. Among the 41 hits, more than half the genes encode metabolic enzymes, including nucleic acid metabolic enzymes CTP synthase 2 (CTPS2) and ribonucleotide reductase regulatory subunit M2 (RRM2), RNA-binding proteins leucine-rich pentatricopeptide repeat containing (LRPPRC) and Ro60, Y RNA binding protein (RO60), protein kinases such as ribosomal protein S6 kinase A5 (RPS6KA5) and mitogen-activated protein kinase kinase kinase kinase 5 (MAP4K5), NRAS proto-oncogene, GTPase (NRAS), ADP ribosylation factor guanine nucleotide exchange factor 2 (ARFGEF2), mitochondrial antiviral signaling protein (MAVS), phosphoribosyl pyrophosphate synthetase 2 (PRPS2), and lysine demethylase 3B (KDM3B). We then overlapped 191 genes downregulated in both *Prrc2b* mouse hearts (at the protein level) and translationally reduced in KO or knockdown human cells (at the TE level) with established PRRC2B-bound mRNAs by us before, together with mouse PDA genes (**Figure 8B**). Seven mRNAs of *PLCG2*, *PHKB*, *WDR26*, *XRCC6*, *TMBIM6*, *PDE12*, and EMC3 are physical PRRC2B-interacting targets reduced at the protein level in *Prrc2b* KO hearts, as uncovered in this study.

Discussion

In this work, we discovered that PRRC2B has two alternative splicing isoforms. Bioinformatic analysis of the PCGC database reveals multiple human mutations of PRRC2B associated with CHD, including p.R1113X. CRISPR-Cas9 mediated introduction of p.R1113X premature termination codon in mouse genome does not cause any apparent cardiac phenotypes at the postnatal stage, possibly due to an intrinsic rescue by an alternative spliced truncated PRRC2B isoform lacking exon 16 (ΔE16). We further demonstrate that *Prrc2b* loss-of-function leads to PDA and, thus, perinatal death in mice (**Figure 8C**). Multiple omics analyses of *Prrc2b* FL and ΔE16 double KO mice suggest changes in SMC number and overall SMC gene expression in the whole heart without significant changes in gene expression in individual, differentiated single SMCs. Genetic knockdown of *Prrc2b* expression in zebrafish using morpholino antisense oligonucleotides causes precardiac edema. Moreover, genetic knockout of the *PRRC2B* gene in human HEK293T cells leads to reduced translation of heart and valve development-related mRNAs, indicating a translational regulatory function of PRRC2B at the molecular level, significantly related to cardiovascular development.

Prior investigations of human cells or mouse models indicate that alternative splicing is a primary intrinsic genetic rescue strategy utilized in cells or tissues to antagonize gene inactivation by genetic manipulation (23). This is consistent with our finding that the human mutation mimicry R1128X KI mice exhibit no apparent cardiac phenotype, likely due to the rescue by ΔE16 isoform expression. Therefore, the R1113X human mutation is unlikely a driver mutation but possibly a modifier mutation, contributing to the CHD phenotypes involving mitral valve abnormality. Alternative splicing of *PRRC2B* pre-mRNA generates two protein isoforms that may have potential functional redundancy that differentiates the phenotypes of *Prrc2b*$^{tm1b-/-}$ versus *Prrc2b* p.R1128X KI mouse models. *Prrc2b* p.R1128X KI mice lost the FL PRRC2B isoform, while the ΔE16 isoform could compensate for the loss-of-function of the full-length protein, thereby maintaining vascular integrity and preventing PDA. This suggests that ΔE16 may partially or fully replace the function of the full-length protein *in vivo*. The evolution of this ΔE16 isoform may serve as a “fail-safe” strategy for the organism to maintain vascular well-being. Exon 16 encodes a domain with RG repeat for RNA-binding, which may not be essential for organismal physiology in mice according to our observations of the viability in the *Prrc2b* p.R1128X KI mouse model. This suggests that additional RNA-binding domains may still exist in PRRC2B. As a supporting hint, mRNA interactome capture analysis identified an mRNA-binding peptide from human PRRC2B (amino acids 385-398 located upstream of the exon 16 spanning amino acids 775-1468) as mapped by

mass spectrometry (6). This peptide is situated very close to the predicted alpha-helix regions (e.g., amino acids 350-370) by Alpha-Fold 2 while far away from the RG-rich domain in exon 16. As an alternative possibility, PRRC2B's RNA-binding and complex-scaffolding functions may be compensated by PRRC2A and PRRC2C, which possess the counterpart RNA-binding domain and show high protein sequence similarity with PRRC2B.

Numerous studies have demonstrated that molecular clues are required for highly coordinated cellular programs to mediate the complex regulation of the DA (24). Notably, functional SMCs are vital for regulating postnatal DA closure after birth (25). To block the blood flow from the pulmonary artery to the aorta and facilitate full activation of pulmonary circulation, the DA vessel needs to be closed rapidly in a short time window after birth, requiring a temporary or spatial surge of protein synthesis for increasing SMC contractility or proliferation locally in the DA vessel areas but not in other blood vessels. When both ΔE16 and FL PRRC2B protein isoforms are absent in *Prrc2b* homozygous KO (tm1b) hearts, SMCs at the DA region may be affected due to compromised translation of specific mRNAs, leading to PDA. The proteomic changes in *Prrc2b* KO hearts suggest translational defects for a selective cohort of proteins triggered by loss-of-function of PRRC2B in the hearts (**Figure 6, 8A, B**). This is consistent with the notion that PRRC2B regulates the translation of a specific group of mRNAs in human cells, as we have reported before (8). Several large-scale unbiased analyses reported that PRRC2B is an RNA-binding protein that can interact with mRNA directly (4-6). Moreover, previous work from Dr. Yamanaka's group and our laboratory uncovered a protein complex of PRRC2B with translation initiation factor eIF4G2 and eIF3 complex in mouse embryonic stem cells or HEK293T cells using mass spectrometry (7,8), implying a conserved composition of PRRC2B-containing complex involved in transcript-selective translational control across different cell types. Our current work on *Prrc2b* KO mice indicates that PRRC2B may play an essential role in cardiac vessel development by regulating temporary and spatial mRNA translation required for optimal proliferation or contraction in local SMCs or other cardiac cell types. Consistent with this idea, *PRRC2B* null HEK293T cells reveal a reduction in the translation of cardiac development-related mRNAs (*BMP2*, *NOTCH1*, *RBPJ*, *ROCK1*, *SNAI2*) (**Figure 7**), highlighting a conserved regulatory program across humans and mice and within different cell types. These findings support a mechanistic link between aberrant cardiovascular development and dysregulated mRNA translation.

Our transcriptomic profiling analysis from E18.5 prenatal *Prrc2b* KO hearts revealed *Myh11* and *Smarca4* downregulation following *Prrc2b* deletion. Since both genes were essential for functional SMCs to orchestrate DA closure, SMC-specific *Smarca4* KO and *Myh11* global KO mice showed

the prevalence of PDA due to insufficient SMC differentiation (*Smarca4* KO) or reduced contractility of SMCs (*Myh11* KO), respectively (26,27). Also, diminished expression of DA closure-related genes (*Acta2*, *Actg2*) responsible for the vascular tone of SMCs (28) was evident in the heart of *Prrc2b*$^{tm1b-/-}$ mice. However, the gene dysregulation at the RNA level is likely a secondary effect downstream of mRNA translational changes. Moreover, snRNA-seq data indicates reduced SMC proliferation or cardiac progenitor cell-to-SMC differentiation. Therefore, we infer that reduced prenatal overall expression of DA-regulating genes upon *Prrc2b* deletion and decreased number of SMCs in the heart may also contribute to the PDA phenotype after birth in addition to compromised mRNA translation.

Taken together, we found that the loss of function of two alternative splicing isoforms of PRRC2B simultaneously caused congenital heart defects (**Figure 8C**). PRRC2B is a novel translation regulatory factor related to cardiovascular development and CHD. Evolving two alternatively spliced isoforms of PRRC2B may be essential for maintaining cardiovascular integrity and species survival. This work provides novel insights for understanding the interplay between alternative splicing regulation of PRRC2B, PRRC2B-mediated translational control, and congenital cardiovascular disorder.

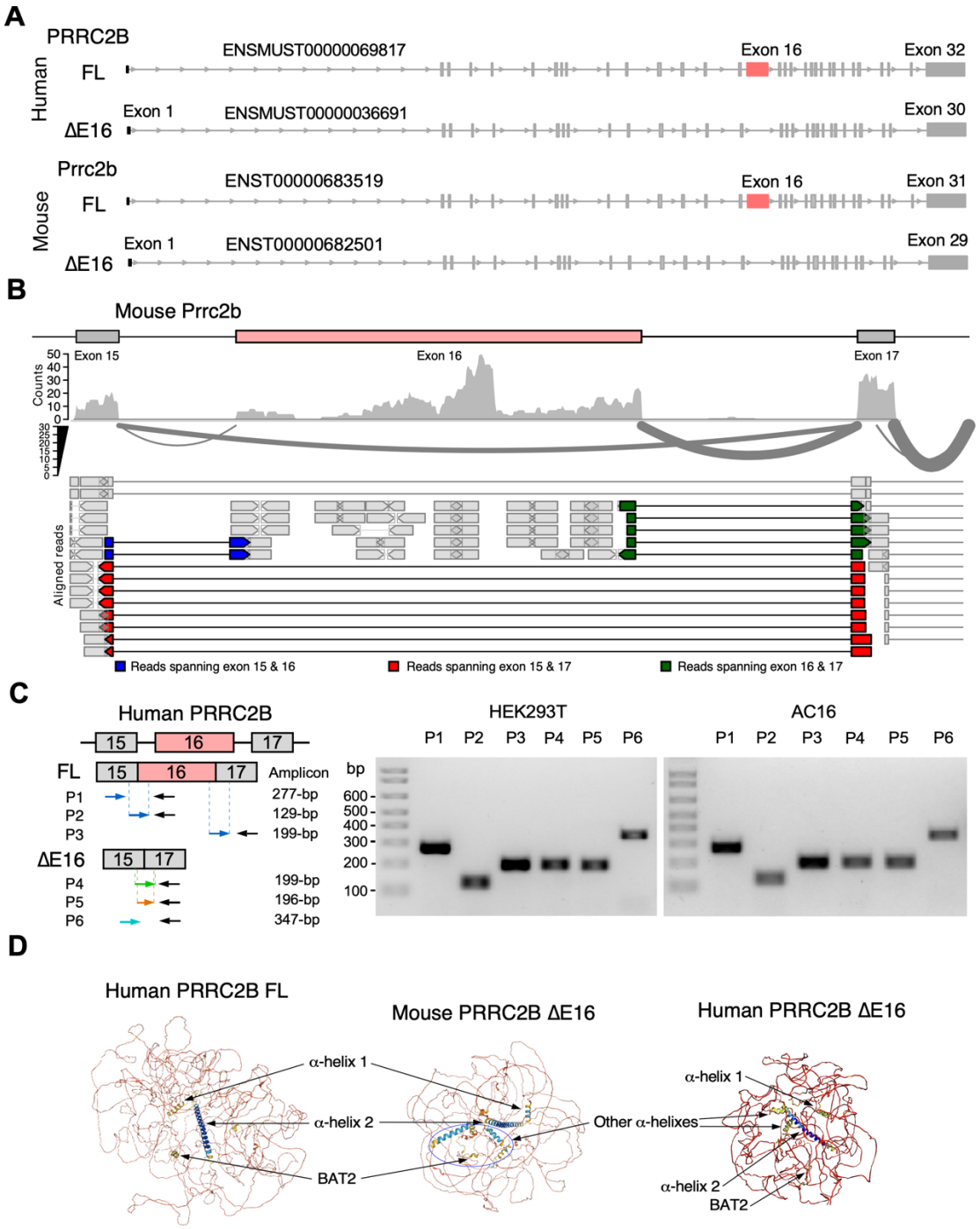

Figure 1. Alternative splicing isoforms of *PRRC2B* mRNA in humans and mice.

A. Schematic of two alternative splicing isoforms of *PRRC2B* mRNA in humans and mice. **B**. RNA-seq reads mapped to exon-exon junction regions at the exons 15-17. Adult hearts from male C57BL/6J WT mice were used for RNA-seq. **C**. RT-PCR validation of alternative splicing isoforms of *PRRC2B* mRNA in HEK293T and AC16 cells. P1-6, primers 1-6. **D**. Predicted protein structure of full-length and ΔE16 PRRC2B in humans and mice by Alpha-Fold.

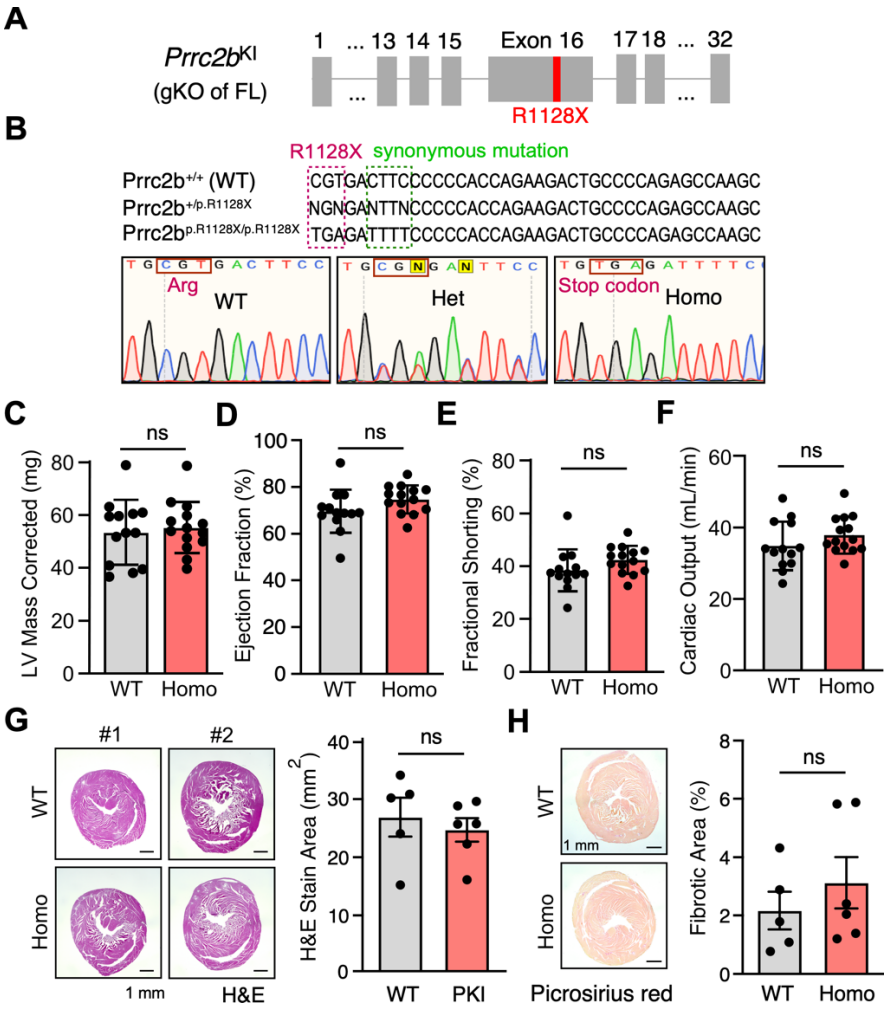

Figure 2. *Prrc2b*$^{R1128X/R1128X}$ knock-in (FL-*Prrc2b*^{gKO}) mice with human genetic mutation of a premature termination codon show inactivation of full-length *Prrc2b* mRNA without causing apparent cardiac phenotypes.

A. Schematic of *Prrc2b*$^{R1128X/R1128X}$ (FL-*Prrc2b*^{gKO}) mouse model. **B**. Sanger sequencing confirms genotyping of the *Prrc2b*$^{R1128X/R1128X}$ (FL-*Prrc2b*^{gKO}) mouse model. **C-F**. LV mass, ejection fraction (EF), fractional shortening (FS), and cardiac output showed no significant difference between WT control and homozygous FL-*Prrc2b*^{gKO} 3 months after birth. WT: N=5M+8F; KO: N=7M+7F. **G**. H&E images of WT and KI mice hearts at 5 months old. Heart size was quantified using Image J. WT: N=3M+2F; KO: N=3M+3F. **H**. Picrosirius red staining of WT and KI mice hearts at 5 months old. The quantification of the fibrotic area for comparison was performed using Image J. WT: N=3M+2F; KO: N=3M+3F. Data are represented as mean ± SD. An unpaired two-tailed Student t-test was performed to compare two groups for C-H. ns: not significant; * $P < 0.05$.

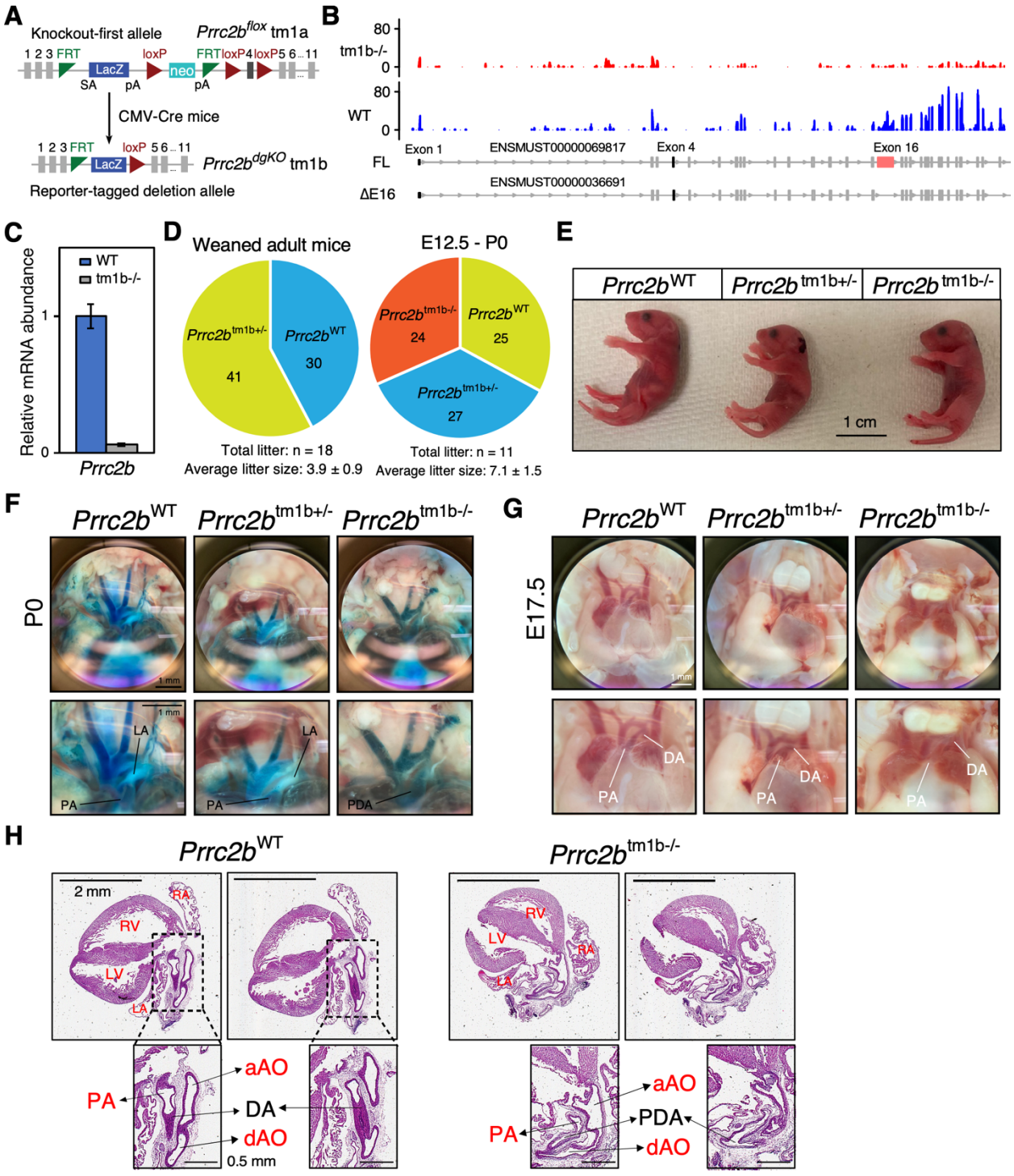

Figure 3. Mice lacking two *Prrc2b* alternative splicing isoforms manifest patent ductus arteriosus (PDA) and die perinatally.

A. Schematic representation of the generation of *Prrc2b* global KO mouse model (*Prrc2b*$^{tm1b-/-}$) by crossing *Prrc2b*^{tm1a} with CMV-Cre mice. Both full-length and ΔE16 *Prrc2b* isoforms are

knocked out. **B**. Integrative Genomics Viewer (IGV) plot of RNA-seq measurement of *Prrc2b* mRNA expression across all the exons. **C**. RT-qPCR analysis of *Prrc2b* mRNA expression in whole hearts of WT and *Prrc2b*$^{tm1b-/-}$ mice. **D**. Number of weaned adult *Prrc2b*^{tm1b} mice and prenatal *Prrc2b*^{tm1b} mice (E12.5 – E18.5) during heterozygous breeding indicated by their respective pie charts. **E**. Images of mice at P0. *Prrc2b*$^{-/-}$ pups were found dead as early as 7 hours postnatally, while *Prrc2b*$^{+/-}$ remained alive. Scale bar: 1 cm. **F**. Images of hearts with Coomassie blue dye injection from WT, *Prrc2b*$^{+/-}$ and *Prrc2b*$^{-/-}$ at P0. Scale bar: 1 mm. PA, pulmonary artery; DA, ductus arteriosus; LA, ligamentum arteriosum; PDA, patent ductus arteriosus. **G**. Images of hearts in the bright field from WT, *Prrc2b*$^{+/-}$ and *Prrc2b*$^{-/-}$ at E17.5. Scale bar: 1 mm. **H**. H&E images of WT and homozygous tm1b KO hearts at P0. LV: left ventricle, RV: Right ventricle, LA: left atrium, RA: right atrium, aAO: ascending aorta, dAO: descending aorta, DA: ductus arteriosus, PA: pulmonary artery, PDA: patent ductus arteriosus.

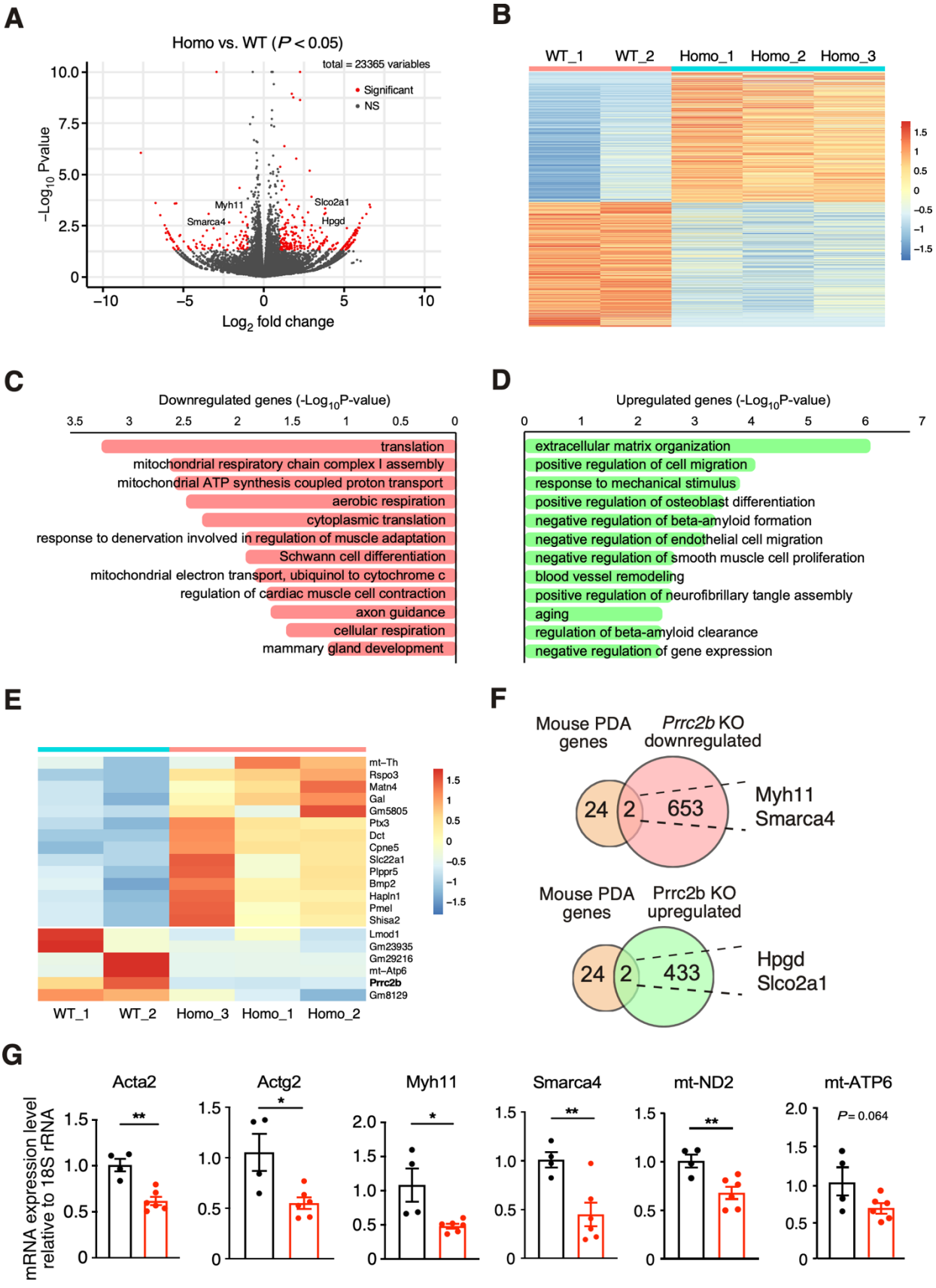

Figure 4. Bulk RNA-seq analysis of Prrc2b global knockout hearts shows reduced smooth muscle cell contraction and mitochondrial respiration-related gene expression.

A. Volcano plot of RNA-seq of WT and *Prrc2b*$^{tm1b-/-}$ hearts at E18.5. Log_2 Fold Change (*Prrc2b*$^{tm1b-/-}$ / WT) is plotted as the X-axis, while -Log10 *P*-values are plotted as the Y-axis. Genes with |Log2 Fold Change| > 1 and *P*-value < 0.05 are colored red. WT: N=2; *Prrc2b*$^{tm1b-/-}$: N=3. **B**. Heatmap of RNA-seq of WT and Prrc2b$^{tm1b-/-}$ hearts. TPM (transcript per million) is plotted. Values are scaled for each row. **C and D**. Gene ontology analysis of upregulated and downregulated genes in RNA-seq of WT and *Prrc2b*$^{tm1b-/-}$ hearts. **E**. A zoomed heatmap showing the top 20 dysregulated genes in (**B**). TPM (transcript per million) is plotted. Values are scaled for each row. **F**. Venn diagrams showing the overlaps between PDA genes and dysregulated genes in *Prrc2b*$^{tm1b-/-}$ hearts. Genes with Log_2 FC > 1 and *P* < 0.05 are considered dysregulated. **G**. RT-qPCR validation of dysregulated genes related to smooth muscle cell contraction and mitochondrial respiratory chain complex in *Prrc2b*$^{tm1b-/-}$ hearts. 18S rRNA is used as the normalizer. Values are plotted as relative values to WT hearts. Data is shown as mean ± SD. Technical replicates for each biological sample are plotted (WT: N=2; *Prrc2b*$^{tm1b-/-}$: N=3). An unpaired two-tailed Student t-test was performed to compare two groups for G. * *P* < 0.05; ** *P* < 0.01.

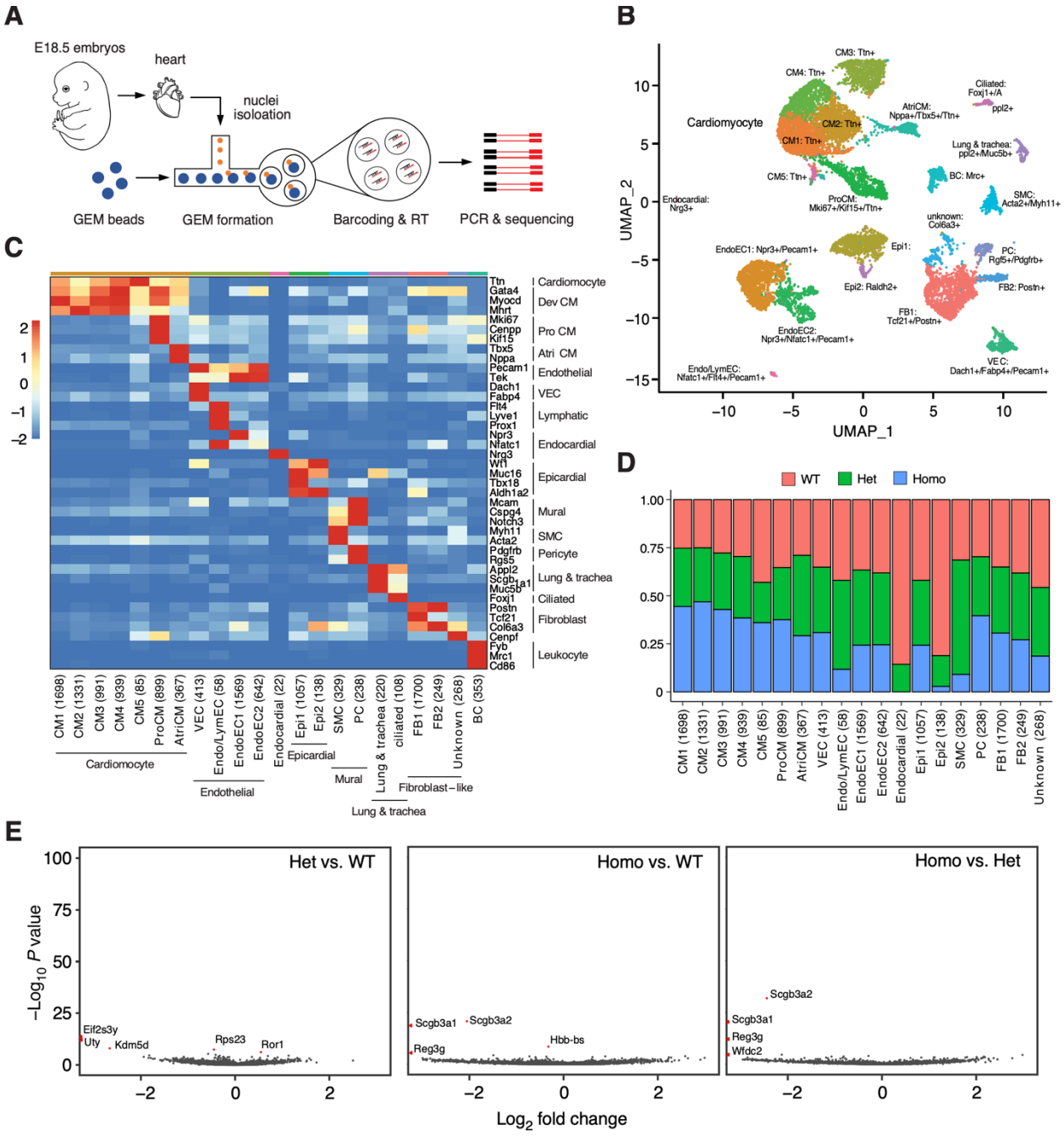

Figure 5. snRNA-seq analysis of *Prrc2b* global knockout hearts.

A. A sketch showing the workflow of snRNA-seq for homozygous *Prrc2b*$^{tm1b-/-}$ gKO, heterozygous *Prrc2b*$^{tm1b+/-}$, and WT control hearts at E18.5. **B**. A UMAP presentation of clustering results based on the top 3000 variant features. 19 clusters were identified and labeled with cell type and top marker genes. **C**. Heatmap showing the expression of well-established marker genes in each cluster. Scaled and normalized expressions were plotted. **D**. A grouped bar plot showing the relative abundance of WT, Het, and Homo cells in each cell type. The Y-axis represents the

fraction of total cells in each cell type. **E**. Volcano plots showing the DEGs in smooth muscle cells. Genes with significantly differential expression (Log_2 FC > 0.2 and Bonferroni correction adjusted $P < 0.05$) were red-colored. Ven.CM, ventricular cardiomyocytes; Atri.CM, atrial cardiomyocytes; FB, fibroblasts; EC, endothelial cells; SMC, smooth muscle cells; BC, blood cells; VEC, vascular EC; Epi, epicardial cells; PC, pericytes; ProCM, proliferating CM; Endo, endocardial; Lym, lymphatic.

A

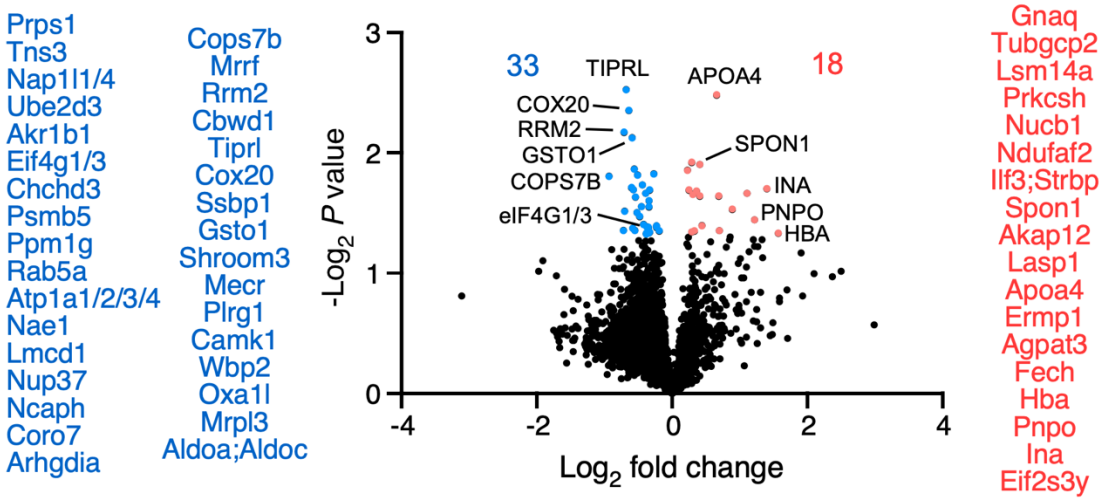

B

Downregulated proteins (P < 0.05)

GO terms	p-value	Genes
Positive regulation of G1/S transition of mitotic cell cycle	2.98×10^{-3}	RRM2, PLRG1, EIF4G1
DNA replication	1.61×10^{-2}	RRM2, NAP1L1, SSBP1
Protein neddylation	2.52×10^{-2}	SHROOM3, CORO7, ALDOA
Mitochondrial respiratory chain complex IV assembly	3.60×10^{-2}	COPS7B, NAE1
Translation	4.37×10^{-2}	OXA1L, COX20
		MRPL3, MRRF, EIF4G1

C

Downregulated proteins ($Log_2FC < -0.75$)

GO terms	p-value	Genes
Mitochondrial translation	4.10×10^{-8}	PTCD3, GFM2, QRSL1, MRPL4, MRPS24...
Mitotic cytokinesis	2.04×10^{-7}	USP8, RASA1, ARL3, UNC119, EXOC5...
Membrane fission	1.10×10^{-5}	VPS4B, VPS4A, MVB12A, CHMP3, EXOC5...
Glycolytic process	3.27×10^{-4}	TIGAR, HKDC1, ENO1, ENO2, ENO3, HK1
Positive regulation of epithelial cell migration	1.52×10^{-3}	GLIPR2, PLCG2, PTK2, CLASP1, CLASP2
Cardiac muscle contraction	2.00×10^{-3}	MAP2K3, GRK2, MYL2, NKX2-5, MYH7

Figure 6. Mass spectrometry analysis of *Prrc2b* global knockout hearts.

A. Volcano plot of differentially expressed proteins identified by mass spectrometry in *Prrc2b*$^{tm1b-/-}$ gKO compared with WT control hearts. 33 downregulated and 18 upregulated proteins with statistical significance ($P < 0.05$) were listed. **B**. Gene ontology analysis of significantly downregulated proteins ($P < 0.05$). **C**. Gene ontology analysis of drastically downregulated proteins ($Log_2FC < -0.75$).

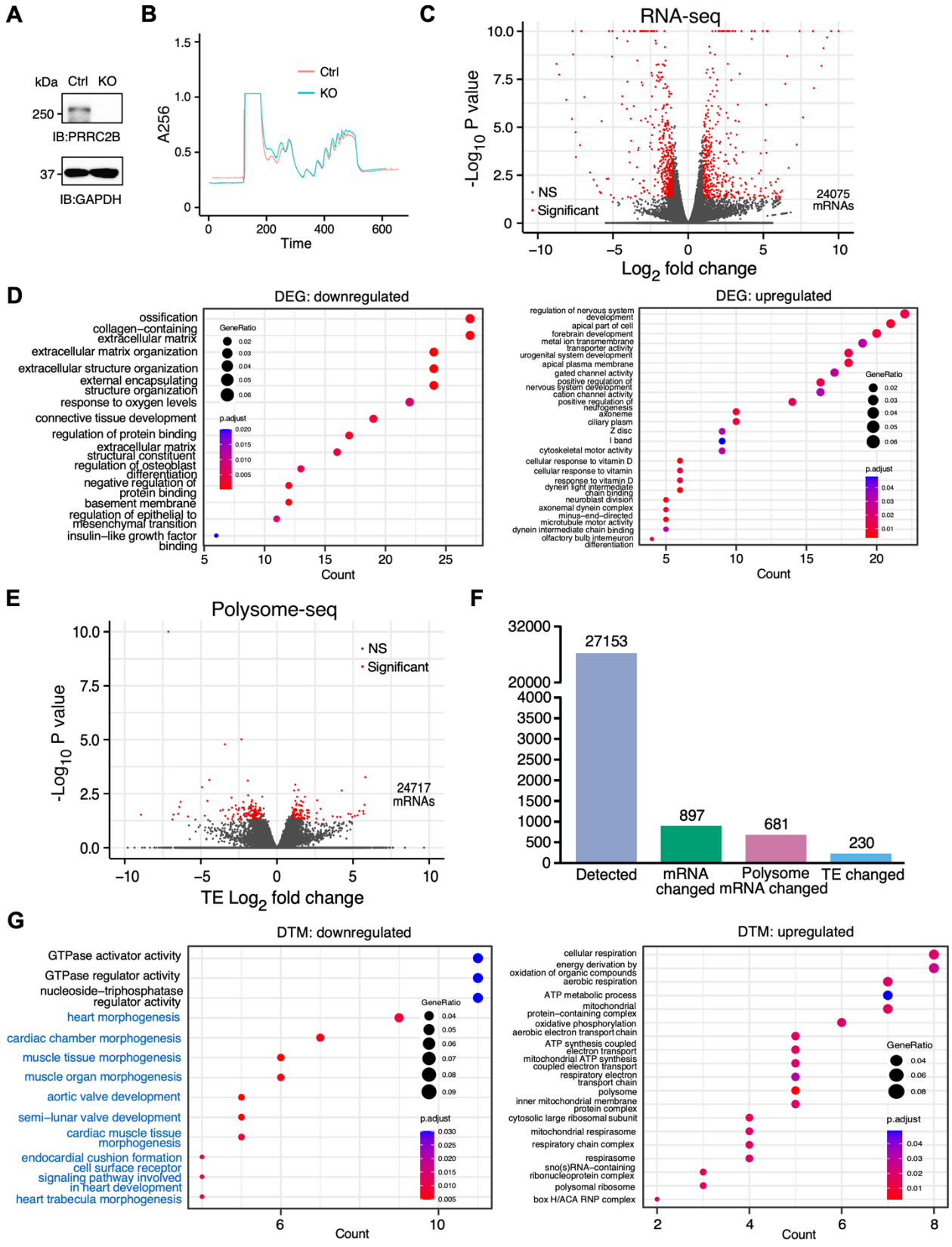

Figure 7. Transcriptomic and translatomic profiling of *PRRC2B* knockout human cells.

A. Immunoblot validation of *PRRC2B* gene knockout in HEK293T cells. **B**. Polysome profiling of control and KO HEK293T cells. **C**. Volcano plot of differentially expressed genes identified by RNA-seq. **D**. GO analysis of significantly downregulated (left) and upregulated (right) genes. **E**. Volcano plot of differentially translated mRNAs (DTM) identified by polysome-seq. **F**. Number of genes significantly dysregulated at the RNA and translation efficiency (TE) levels in KO cells. **G**. Gene ontology analysis of significantly TE-downregulated (left) and -upregulated (right) mRNAs. DTM-downregulated pathways are highlighted in blue.

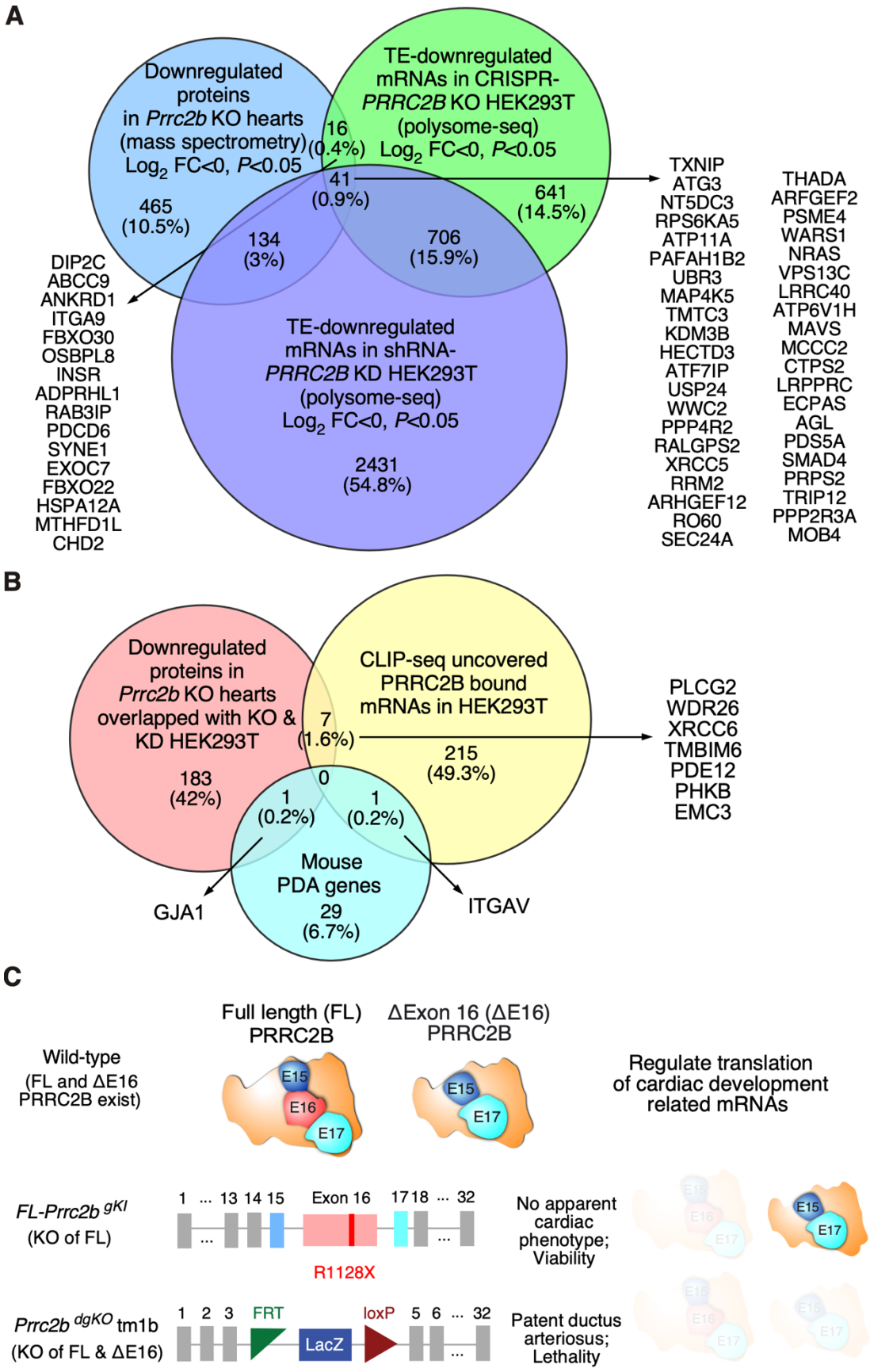

Figure 8. Conserved PRRC2B-regulated target mRNAs across cell types and species.

A. Venn diagram of shared PRRC2B-regulated genes from *Prrc2b*$^{tm1b-/-}$ gKO mouse hearts and *PRRC2B* KO and KD human HEK293T cells. Conserved downregulated genes at the protein translation level are listed. **B**. Venn diagram of overlapping reduced proteins in *Prrc2b*$^{tm1b-/-}$ KO mouse hearts with PRRC2B-bound mRNAs from human cells and well-known mouse PDA genes. Conserved downregulated genes at the protein translation level are listed. **C**. Schematic model showing the two alternative spliced *PRRC2B* isoforms (FL and ΔE16) and phenotypes of the *Prrc2b* genetic mouse models.

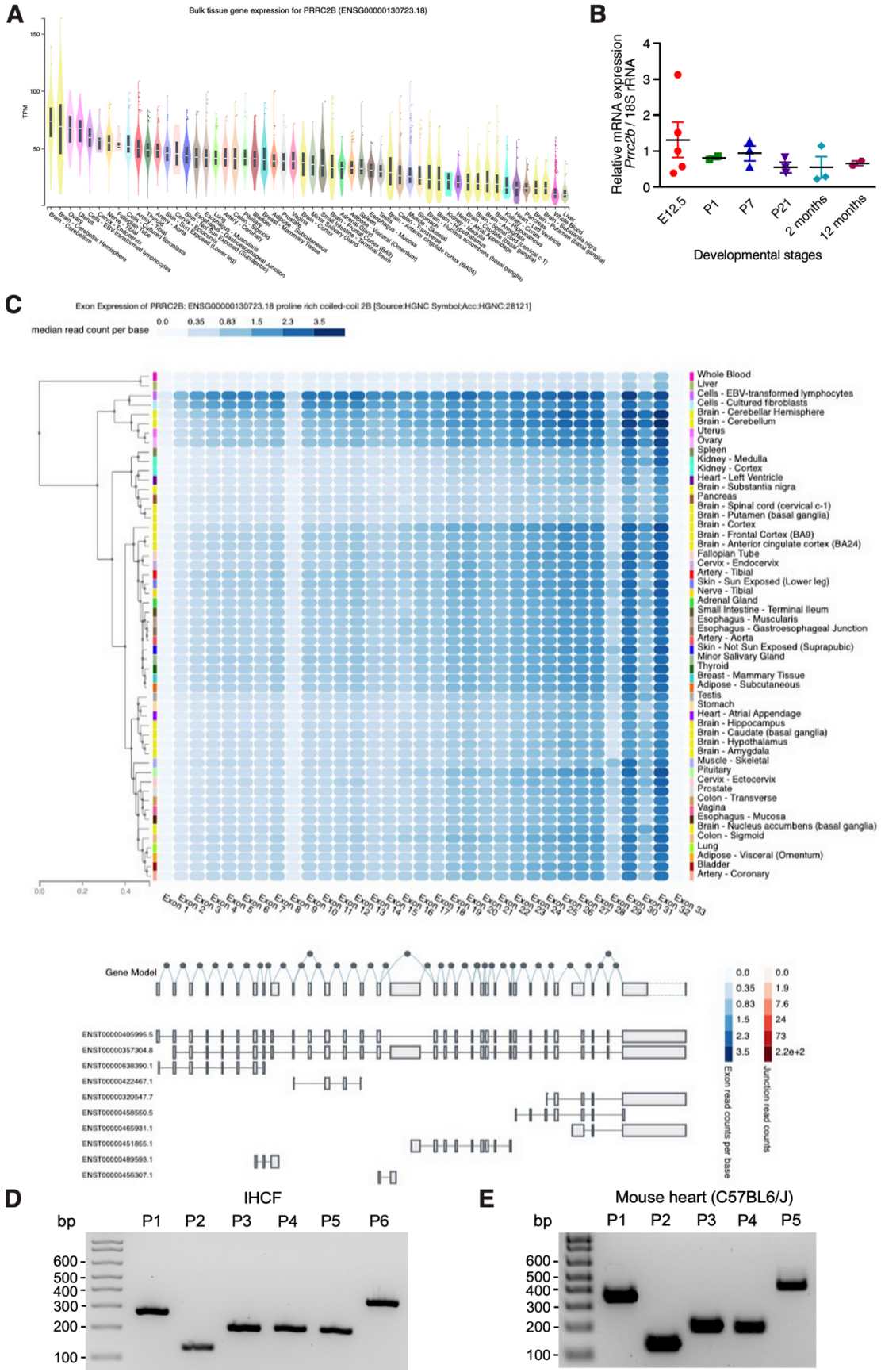

Figure S1. Alternative splicing patterns of *PRRC2B* in human organs.

A. Bulk tissue gene expression for *PRRC2B* mRNA in human organs from GTEx Portal databases. **B**. *Prrc2b* mRNA expression in mouse hearts at different developmental stages. **C**. Alternative splicing isoforms of *PRRC2B* mRNA across different human organs. **D**. RT-PCR validation of alternative splicing isoforms of *PRRC2B* mRNA in IHCF cells. P1-6, primers 1-6. **E**. RT-PCR validation of alternative splicing isoforms of *Prrc2b* mRNA in the mouse heart (from 2 months old C57BL6/J male mouse). P1-5, primers 1-5.

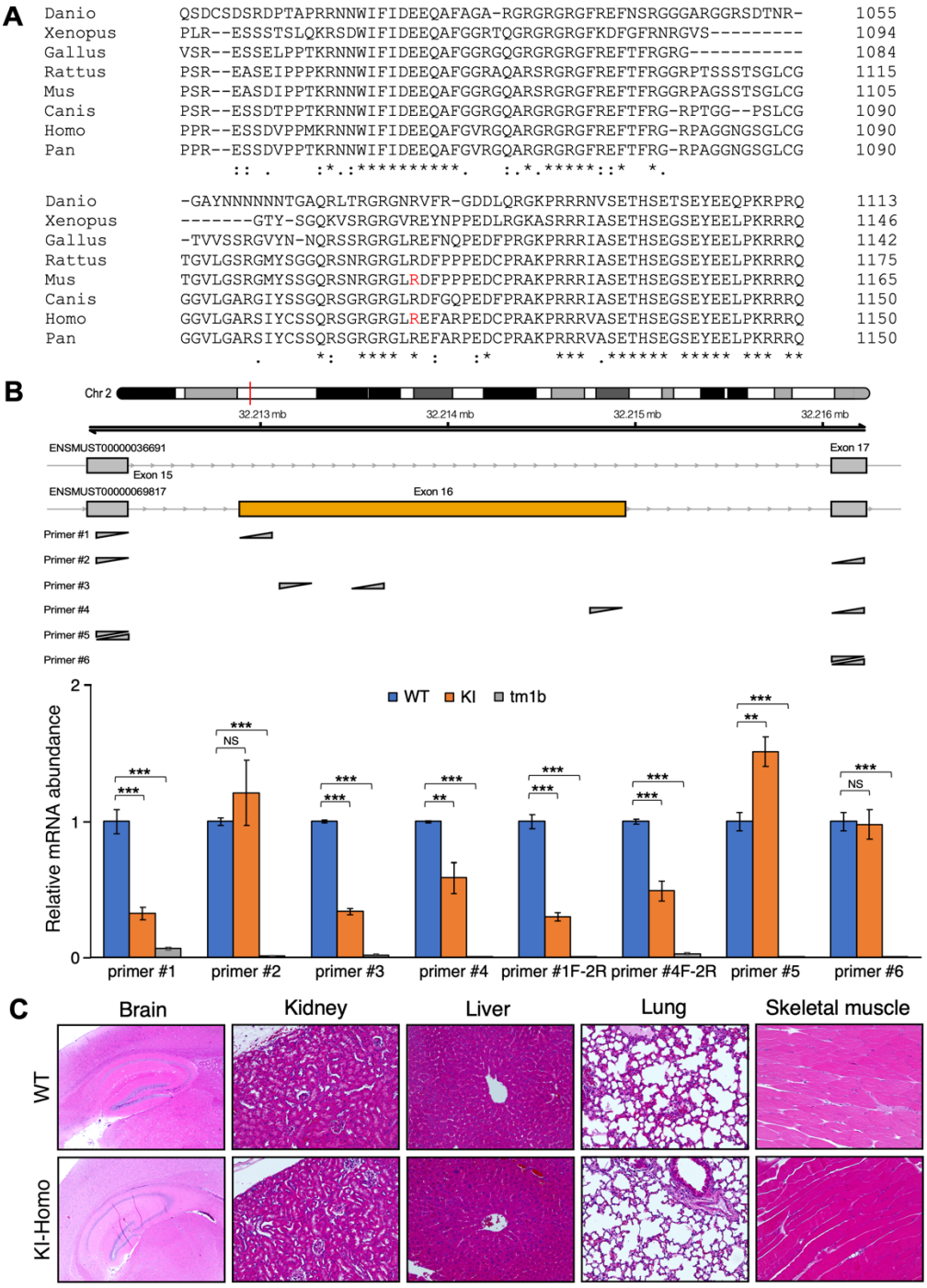

Figure S2. Characterization of *Prrc2b*$^{R1128X/R1128X}$ global knock-in mice

A. Evolutionary conservation of PRRC2B protein sequence surrounding the R1113 amino acid residue in humans across various species (R1128 in mice). **B**. RT-qPCR detection of alternative splicing isoforms of *Prrc2b* mRNA in *Prrc2b*$^{R1128X/R1128X}$ global knock-in (FL-*Prrc2b*^{gKO}) and tm1b (*Prrc2b*^{gKO}; KO of both FL and ΔE16 alternative spliced isoform of *Prrc2b* mRNAs) mice. **C**. Representative H&E images of multiple organs of WT and *Prrc2b*$^{R1128X/R1128X}$ global knock-in mice.

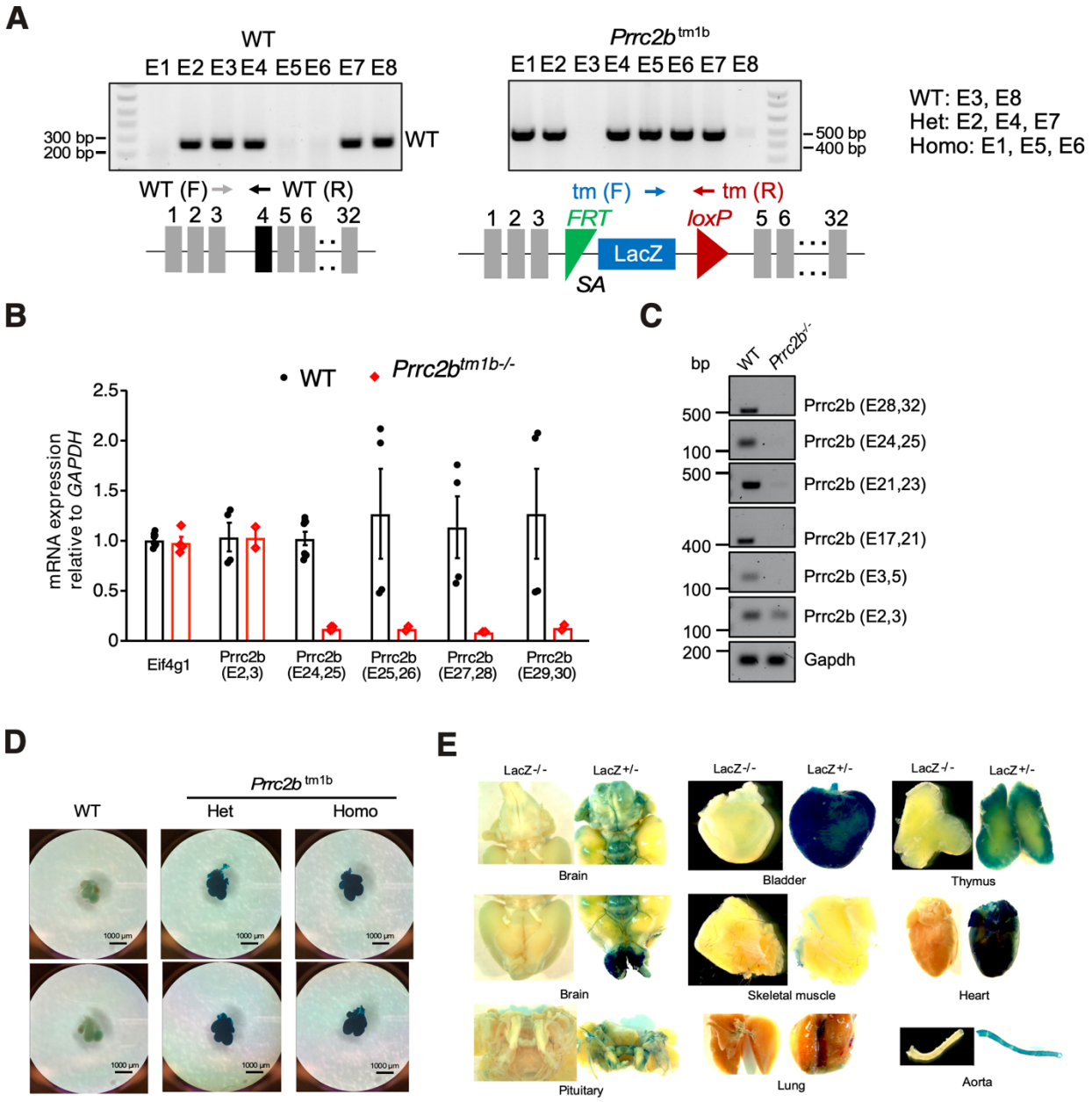

Figure S3. Generation of *Prrc2b*^{tm1b} global knockout mice (*Prrc2b*$^{-/-}$).

A. Representative genotypes of *Prrc2b*$^{-/-}$, *Prrc2b*$^{+/-}$ and *Prrc2b*^{WT} at E13.5 determined by two pairs of primers (6tm, F and 7tm, R) and (WT, F and WT, R). **B**. Representative agarose gel electrophoresis of PCR products from cDNA harvested from heart were determined by two pairs of primers (Ex2, F and Ex3, R), (Ex3, F and Ex5, R), (Ex17, F and Ex21, R), (Ex21, F and Ex23, R), (Ex24, F and Ex25, R) & (Ex28, F and Ex32, R) and normalized with the housekeeping gene, *Gapdh*. **C**. RT-qPCR measurement of *Prrc2b* mRNA expression normalized by *Gapdh* mRNA. **D**.

LacZ staining of embryonic hearts at E12.5. **E**. LacZ staining of multiple organs in WT and *Prrc2b*$^{+/-}$ adult mice.

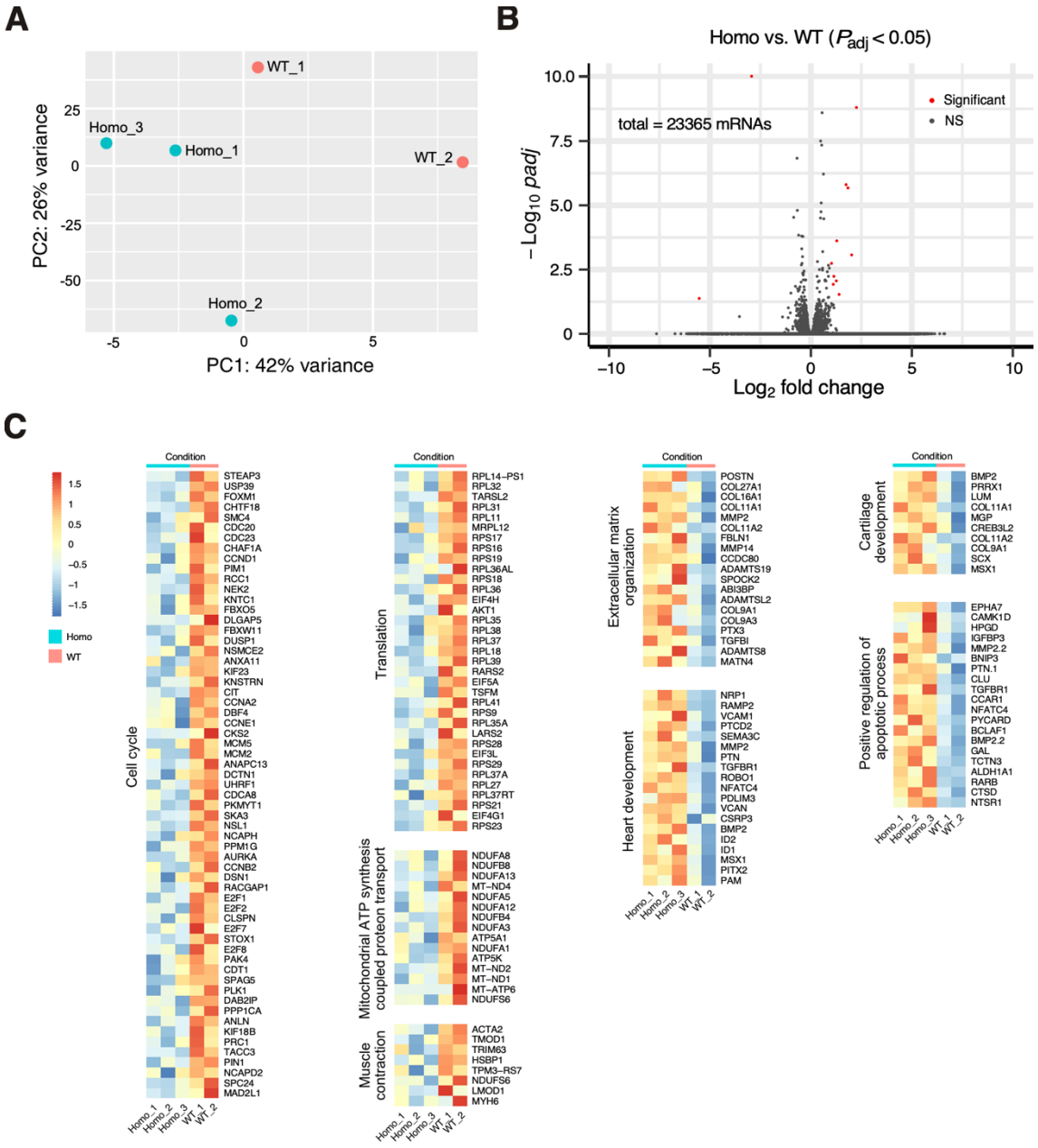

Figure S4. RNA-seq analysis of *Prrc2b* global knockout hearts

A. PCA component analysis of RNA-seq data for WT and Homozygous *Prrc2b* tm1b KO hearts. **B**. Volcano plot of RNA-seq of WT and *Prrc2b*$^{tm1b-/-}$ hearts. Log_2 Fold Change (*Prrc2b*$^{tm1b-/-}$ / WT) is plotted as the X-axis while -Log10 P_{adj}-values are plotted as the Y-axis. Genes with |Log2 Fold Change| > 1 and P_{adj}-value < 0.05 are colored red. **C**. Heatmap of differential gene expression for multiple GO pathways.

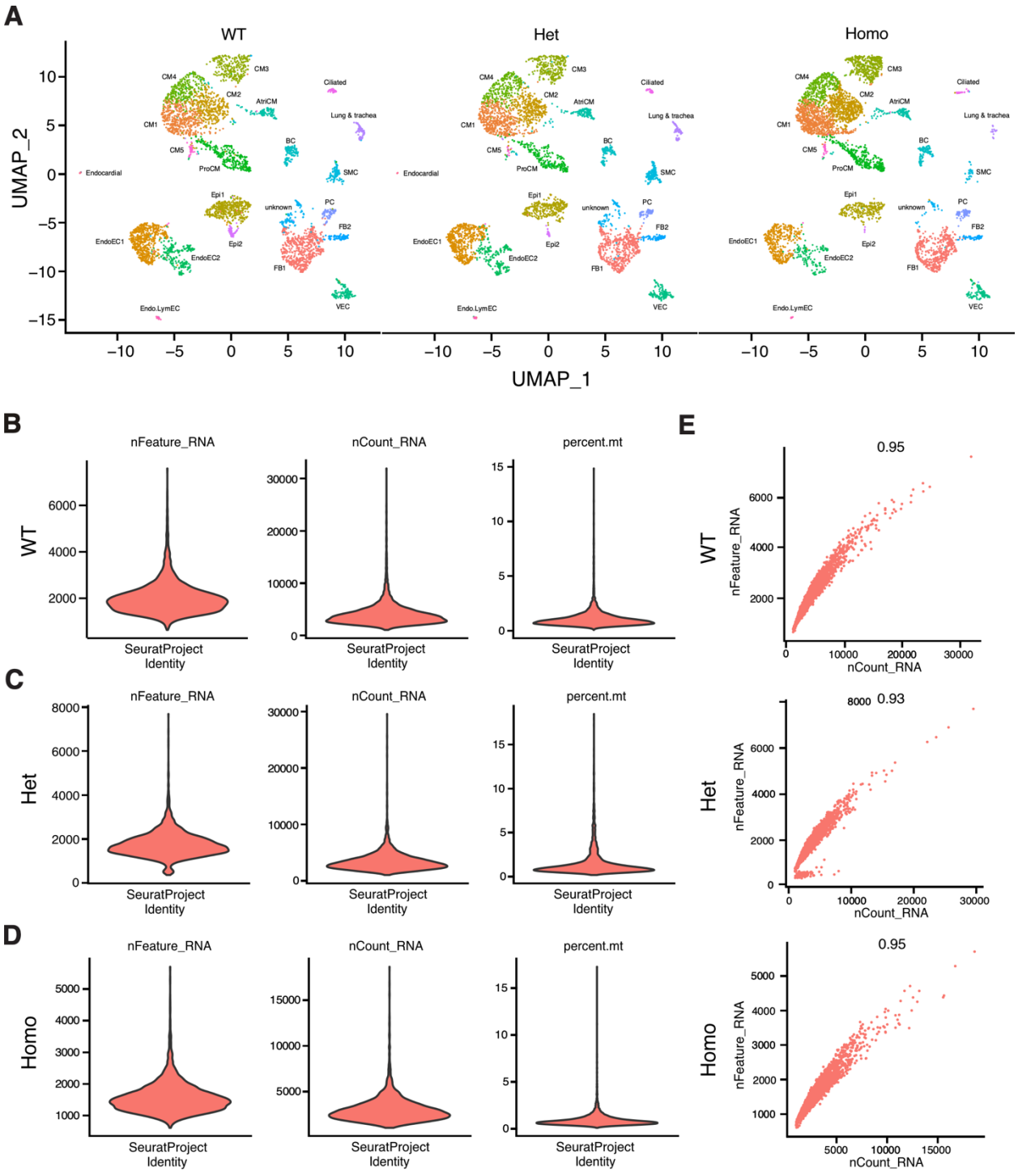

Figure S5. snRNA-seq analysis of *Prrc2b* global knockout hearts

A. A UMAP presentation of clustering results based on the top 3000 variant features. 19 clusters were identified and labeled with cell type and top marker genes. Nucleus from WT, HET, and HOMO were clustered together and plotted separately. Ven.CM, ventricular cardiomyocytes; Atri.CM, atrial cardiomyocytes; FB, fibroblasts; EC, endothelial cells; SMC, smooth muscle cells;

BC, blood cells; VEC, vascular EC; Epi, epicardial cells; PC, pericytes; ProCM, proliferating CM; Endo, endocardial; Lym, lymphatic. **B-D**. Quality control vlnplots showing the distribution of number of genes (nfeature) (**B**), number of reads (ncount) (**C**), percentage of mitochondrial coded genes (percentage.mt) (**D**) detected in each nucleus in each mouse heart (WT, HET, HOMO). **E**. Quality control scatterplots showing the number of genes (nfeature, y-axis) and the number of reads (ncount, x-axis) detected in each nucleus in each sample. Pearson correlation coefficient is labeled.

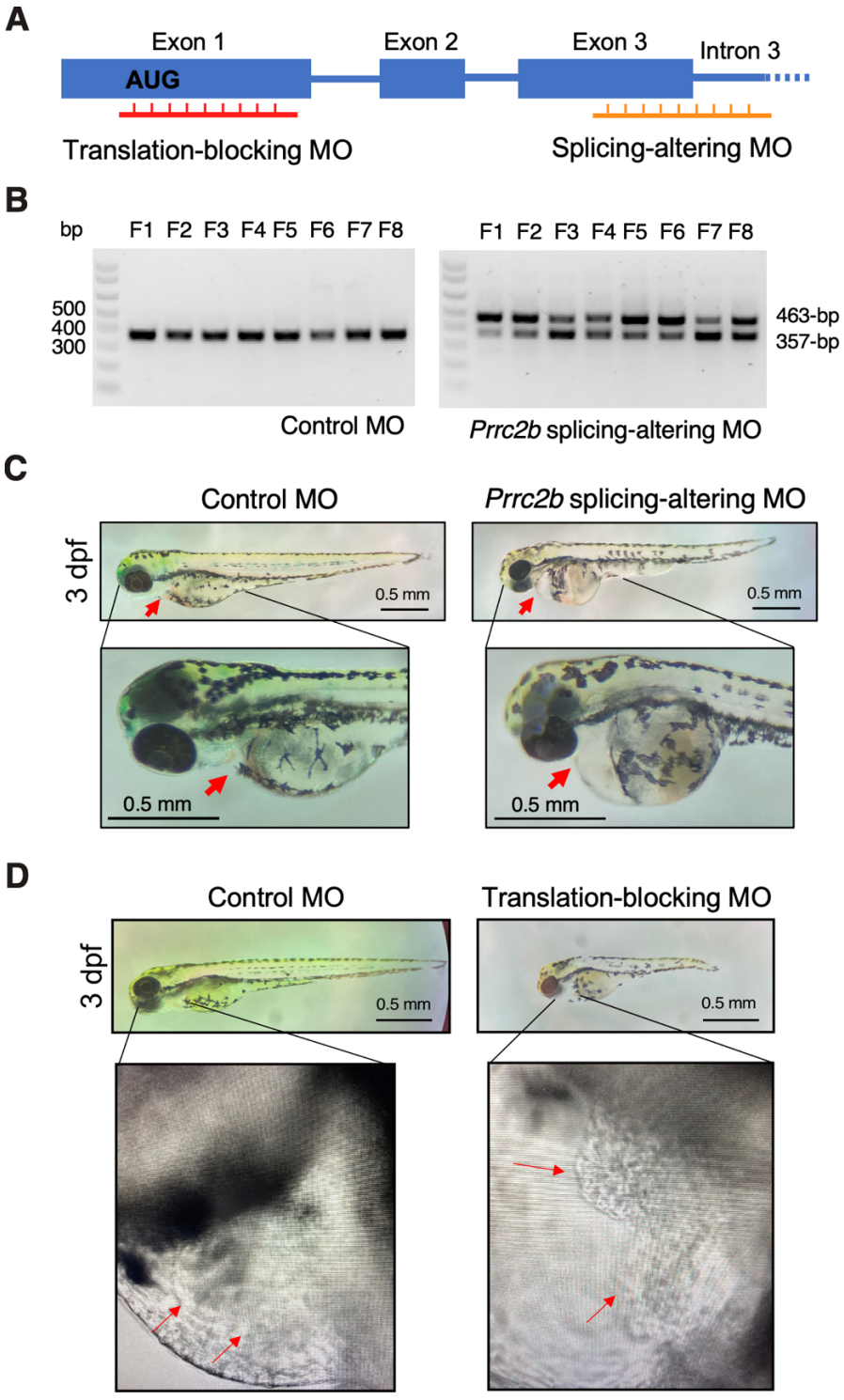

Figure S6. Cardiac developmental defects in zebrafish upon ASO-mediated *Prrc2b* inactivation.

A. Schematic of *Prrc2b*-inactivating antisense morpholino oligomers (MO). Translation-blocking MO inhibits the translation of *Prrc2b* mRNA. Splicing-altering ASO either skips exon 3 or includes

intron 3. **B**. Representative agarose gel electrophoresis images of PCR products from cDNA upon RT of total RNA harvested from control MO- and *Prrc2b* splicing-altering MO-injected embryos determined by primer pair (e1E2, F & E4e5, R). **C**. *Prrc2b* splice-exon3 MO was injected into 1–4 cell stage in zebrafish embryos to cause aberrant *Prrc2b* mRNA splicing and nonsense-mediated mRNA decay. A total of five *Prrc2b* splicing-altering MO-injected embryos showed curved bodies with pericardial edema. Representative images were shown. Scale bar: 0.5 mm. **D**. *Prrc2b* translation-blocking MO was injected into 1–4 cell stage in zebrafish embryos to inhibit *Prrc2b* mRNA translation. A total of four translation-blocking MO-injected embryos showed curved bodies with pericardial edema. Representative images were shown. Scale bar: 0.5 mm.

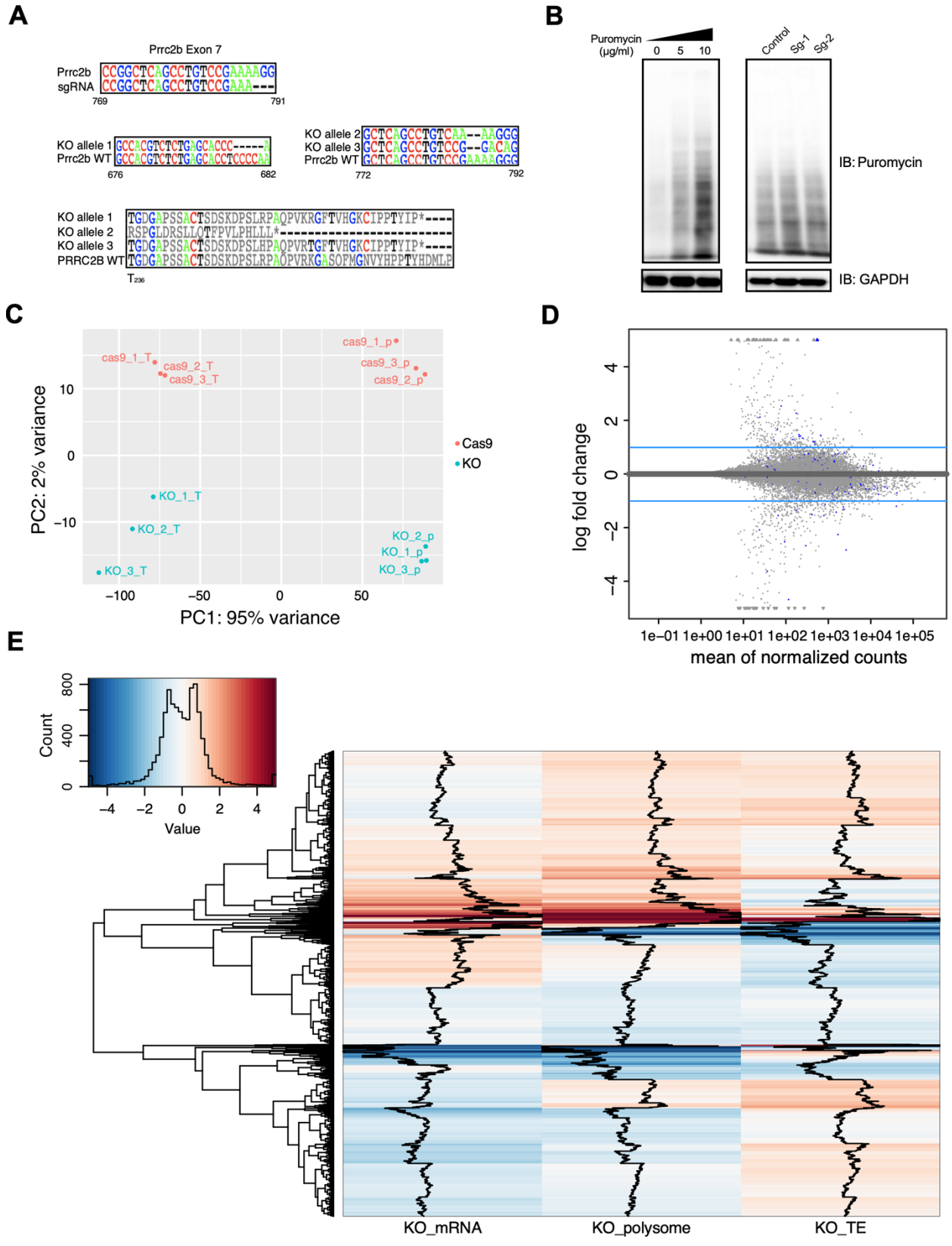

Figure S7. Transcriptomic and translatomic profiling of *PRRC2B* knockout human cells. **A**. Sanger-sequencing of DNA locus of three copies of *PRRC2B* gene in KO HEK293T cells. **B**. Puromycin incorporation assay of control and KO HEK293T cells. Sg1 and Sg2 are two single gRNAs for KO. **C**. PCA analysis showing the distribution of the biological triplicates of RNA-seq (T) and polysome-seq (p) for the control and KO cells. **D**. An M (log ratio) versus A (mean average) plot (MA-plot) showing the distribution of differentially expressed genes. Genes with significant *P* values ($P < 0.05$) are colored in blue. **E**. Heatmaps for RNA-seq and polysome-seq and calculated TE showing the annotated dysregulated genes in all samples. The black lines indicate the average fold change per gene across the dataset.

Materials and methods

Whole exome sequencing and burden testing for published PCGC databases

Results of genomic analysis using the pediatric cardiac genomic consortium (PCGC) whole exome cohort have previously been published (18), and the analysis here follows previously described protocols (12,29,30). Briefly, whole exome DNA from blood or salivary samples was captured using the Nimblegen v.2 exome capture reagent (Roche) or Nimblegen SeqxCap EZ MedExome Target Enrichment Kit (Roche), followed by Illumina DNA sequencing as previously described (12,29,30). The data generated was processed at Yale University School of Medicine and reads were mapped to the hg19 reference genome. Mapped reads were further processed using the GATK Best Practices workflows (31), as previously described (29). Single nucleotide variants and small indels were called with GATK HaplotypeCaller (32). Further filtering of the data set was performed using PLINK (33), including removing individuals with low call rates, outlying heterozygosity rates, outlying relatedness rates, and sex discrepancy. A total of 3,740 probands passed individual filtering (18). Variants were filtered on call rate, Hardy-Weinberg equilibrium, and a high number of Mendel errors (≥3). Variants within PRRC2B were extracted using the longest known canonical hg19 PRRC2B variant bed file downloaded from UCSC Table Browser on 9/19/2021 (34). The remaining variants were annotated using ANNOVAR (35). Loss of function (frameshift, splice site, start lost, stop gained, and stop loss) and missense variants with a CADD (36) score >20 and a minor allele frequency <0.001 in all gnomAD (37) populations were kept for burden analysis. Dichotomous traits were created by comparing probands with a specific phenotype to the rest of the probands in the PCGC whole exome cohort. Burden testing using these dichotomous traits was completed using the sequence kernel association test (SKAT) (38) package in R with the first three principal components as covariates.

Generation of *Prrc2b* knockout mice (*Prrc2b*$^{Tm1b-/-}$)

Prrc2b$^{tm1b-/-}$ mice were generated using the knockout-first strategy. The detailed schematic representation of the targeted *Prrc2b* allele is illustrated in **Figure 3A**. The Prrc2b targeting vector (PG00197_Z_2_F04) was obtained from the Knockout Mouse Project Repository (IKMC project: 71689). Heterozygous knockout-first (*Prrc2b*^{tm1a}) mice containing promoter-driven cassette (L1L2_Bact_P) which was inserted at position 32074888 of Chromosome 2 upstream of the critical exon four of *Prrc2b* gene. Then, *Prrc2b*^{flx} Tm1a mice were mated with Tg (CMV-Cre) mice to generate an exon four knockout allele (*Prrc2b*^{gKO} tm1b) **(Figure 1)**. The PCR primers used for genotyping to validate the knockout alleles are summarized in **Table S6**.

Generation of *Prrc2b* R1128X knock-in mice

Prrc2b global R1128X knock-in (KI) mice were generated by the Mouse Genome Editing Resource at URMC using the CRISPR-Cas9 method. The guide RNA (gRNA) used for *Prrc2b* KI was designed using an online CRISPR RNA design tool developed by Dr. Feng Zhang's lab (http://crispr.mit.edu). The gRNA with the highest score and lowest off-target probability was chosen. The efficiency of gRNA and Cas9-2xNLS (Synthego) were tested in a tube *in vitro* using a 500-bp mouse genomic DNA-derived PCR product that contains the target sequence. Then, 25 pmol of single guide RNA (sgRNA) and 25 pmol of Cas9 nuclease were mixed in the injection buffer in a 12.5 μl reaction. The mixture was then incubated at room temperature for 10 min to form the RNP complex. Finally, this RNP complex was mixed with a single-strand DNA template that contains Arg codon-to-stop codon at the position of 1128 amino acid and two additional wobble base mutations (GACTTC-to-GATTTT) at 1:3 molar ratio for pronuclear injection. In this project, injected embryos were transferred into multiple recipient C57/BL6J mice, and we obtained mosaic pups containing desired mutations. To get the heterozygous gKI mice for experiments, mice from injection were bred with C57BL/6J WT mice for germline transmission. They kept breeding with WT mice for 5 generations to remove the potential off-target sites. The genotyping was conducted by Sanger sequencing of the PCR amplified fragments covering the WT versus the gKI mutation regions.

Guide RNA (20 nt):

5' CCCUGCCUCGGUUACUGCGC 3'

DNA template (194 nt):

GCAGGCAGCAGCACAAGTGGTCTTTGTGGCACGGGTGTCCTTGGGTCTCGTGGCATGTAC
AGTAGTGGGCAGCGCAGTAACCGAGGCAGGGGCCTGTGAGATTTTCCCCCACCAGAAGA
CTGCCCCAGAGCCAAGCCAAGGCGTCGCATTGCCAGCGAGACTCACAGCGAGGGCTCTG
AGTATGAAGAGCTGCC

Perinatal mouse heart isolation

Prrc2b$^{tm1b+/-}$ mice were set up in the evening for timed mating to harvest the embryos from the exact day of gestation, ranging from E12.5 (prenatal stage with fully developed heart) to P0 (early postnatal stage). The plug (white to yellowish ejaculate) was checked early in the morning to detect pregnancy signs. Once pregnancy was confirmed, their body weights were recorded regularly until the desired stage for harvest. For prenatal stage harvesting, the pregnant mice were euthanized with a mixture of ketamine and xylazine via intraperitoneal (IP) injection.

Individual embryos were extracted from the uterus, followed by heart isolation under the dissection microscope. They were immersed in prechilled 1X PBS buffer to wash out the excessive blood before isolating the hearts. Whereas, for early postnatal stage (P0) harvesting, the pregnant mice were closely observed for the exact delivery date and time. Then, the freshly delivered fetuses were separated and euthanized with rapid freezing. The mouse sternum was dissected, and the heart was exposed before perfusing with 1X PBS buffer before isolating the heart.

Total RNA extraction

Total RNAs were harvested from heart tissues of neonatal mice (P0) using TRIzol reagent (Thermo Fisher). Briefly, the heart tissues in 500 ul of TRIzol were homogenized for 1 min using the Precellys kit (Bertin Technologies) on the Minilys® Personal Homogenizer (Bertin Technologies). Then, the homogenates were placed on ice for 10 mins to allow for complete lysis. Then, 100 μl of chloroform was added to the homogenates, followed by vigorous shaking by hand for 15 secs, and incubated for 5 mins at room temperature. The mixture was centrifuged to allow separation into a lower phenol: chloroform phase, an interface, and an upper aqueous phase. The upper layer was transferred to a fresh tube, followed by 500 μl of isopropanol and 2 μl of 20 mg/ml glycogen for precipitation. After centrifugation, the pellet was washed once with 75% ethanol, followed by another centrifugation to obtain the RNA pellet.

mRNA expression by agarose gel electrophoresis of cDNA after PCR

After RNA isolation, 1 μg of total RNA was used as the template for reverse transcription using SuperScript^{TM} IV RT (Invitrogen) following the manufacturer's instruction. cDNA was then obtained to detect the mRNA expression of *Prrc2b* at different exon positions. *Gapdh* was used as a housekeeping control. Then, the PCR products were loaded in 1.5% agarose gel and run at 140 V for 30 mins before visualization.

RNA-sequencing analysis and data processing

As aforementioned, total RNAs were harvested from WT and *Prrc2b*$^{tm1b-/-}$ mice. Another step was added to prevent potential genomic DNA contamination in the isolated RNA. To do so, the RNA pellet was treated with DNase I (NEB) and incubated for 10 mins at 37^{o}C. Next, 50 mM EDTA solution was added to the digested RNA solution and incubated for 5 mins at 65^{o}C to stop the digestion. Repurification was performed with 100 μl of phenol/chloroform/isoamyl alcohol (25:24:1). Next, the upper layer was transferred to a fresh tube, followed by adding 10 μl of 3M sodium acetate, 2 μl of glycogen, and 250 μl of absolute ethanol to allow RNA precipitation. Lastly,

the pellet was washed once with 75% ethanol followed by another centrifugation to obtain the RNA pellet. PolyA enrichment was performed before library construction by NGS Library Prep. Paired-end sequencing was conducted at Novogene using NovaSeq 6000 S4 with a depth of 20 million reads/sample. Reads were demultiplexed using bcl2fastq version 2.19.0. Quality filtering and adapter removal were performed using Trimmomatic version 0.36 (39) with the following parameters: "ILLUMINACLIP:2:30:10 LEADING:3 TRAILING:3 SLIDINGWINDOW:5:25 MINLEN:32 HEADCROP:10". Processed/cleaned reads were then mapped to the Homo sapien reference genome (GRCh38, hg38) with Hisat version 2.1.1 (40) with the default settings. The subread-2.0.1(41) package (featureCounts) was utilized to derive gene counts using the gencode.v38 gene annotations (42) with the following parameters: "-T 10 -g gene_name -B -C -p --ignoreDup --fracOverlap 0.1". DESeq2 version 1.38.3 (43) was used within an R-4.2.2 (44) (URL: https://www.R-project.org/) environment to normalize raw counts and identify significantly changed genes. Gene ontology analyses were performed on significantly changed genes using clusterProfiler package version 4.6 (45).

Single-nucleus RNA-sequencing analysis

Single-nucleus RNA-sequencing (snRNA-seq) was carried out by SingulOmics Corporation following their established protocols. Whole hearts were harvested from both WT and *Prrc2b*$^{tm1b-/-}$ mice, which were at an age of E18.5 (n = 3), and were fast frozen in liquid nitrogen. Nuclei were isolated from the frozen mouse heart tissue using the 10x Genomics single nuclei isolation kit, adhering to the manufacturer's instructions. The snRNA-seq libraries were constructed using the 10x Genomics Chromium System and the 10x Chromium Multiome kit. Each library was subjected to sequencing on the Illumina NovaSeq 6000 platform, generating approximately 200 million paired-end reads (PE150) per library. snRNA-seq reads were demultiplexed and aligned to mouse reference genome mm10 by 10x Genomics Cell Ranger ARC 2.0.2 [27]. A count matrix was created by summarizing reads mapped to both exon and intron regions of each gene in each nucleus.

Dimension reduction, clustering, annotation, and differential expression analysis

Only nuclei with more than 200 snRNA-seq reads fragments were included in the analysis. Potential doublets were eliminated using DoubletFinder [28], with an estimated doublet rate of 5%. Dimension reduction and clustering primarily relied on the top 3000 variant features in snRNA-seq data. Before these processes, data from WT and KO hearts were integrated together, utilizing SCTransformed[29] counts and relevant functions in Seruat v4[30] in an R-4.2.2 environment. Dimension reduction was initiated with a PCA test, with a subsequent UMAP test utilizing the first

20 PCs. Clustering was performed via the k-nearest neighbors algorithm and Shared Nearest Neighbor (SNN) algorithm [31]. Cluster annotations were initially established by comparing gene expression profiles to publicly available annotated datasets using SingleR [32], with gene expression counts normalized and scaled before these comparisons. Reference datasets from Tabula Muris [33], containing snRNA-seq data from mouse heart and aorta, were employed for this annotation, and additional refinement was undertaken by considering normalized RNA expression and gene accessibility data for well-established cardiac cell-type-specific markers [34,35]. To identify differentially expressed genes (DEGs) within each cluster, a logistic regression model, known for its robust performance in previous work [36], was applied to the normalized counts, with variations in sequencing depth among the nucleus being treated as latent variables. The DEG analysis included only genes expressed in more than 10% of the cluster. Bonferroni correction was applied to adjust the nominal *P* values; genes with |Log2 fold change| > 0.2 and adjusted $P < 0.05$ were considered significant.

Zebrafish maintenance and microinjection of morpholinos

Adult and larval zebrafish husbandry and care were conducted in full accordance with animal care and use guidelines with ethical approval by the University Committee on Animal Resources at the University of Rochester Medical Center. Adult wild-type Tübingen zebrafish were maintained on a 14h: 10h (light: dark cycle), and newly fertilized embryos were collected and used for morpholino injection and phenotypic characterizations. Morpholinos were designed against the 5'-terminal sequence near the start codon (ATG) and the junction of exon 3 intron 3 (e3i3) of the *Prrc2b* gene to block mRNA translation and trigger exon 3 exclusion, respectively. *Prrc2b* MO (Trans Morpholino): 5'-ATTTGCCCCAAACGATCGGACATTG-3'; *Prrc2b* MO (e3i3 Morpholino): 5'-TACAACACACACGCCGTACCTCC-3'; and a standard control MO (5'-CCTCTTACCTCAGTTACAATTTATA-3') were injected into one to two cell-stage of zebrafish embryos. Images of zebrafish larvae were taken using a dissecting microscope.

Table S1. PRRC2B Variant Burden Test in CHD probands

Phenotype (N)	Gene Wide Burden	Variants at RNA binding sites	Variants at arginine sites	Gene Wide Burden: Ultrarare
LVOTO (863)	0.14133	0.08867	0.28310	0.31683
HLHS (399)	0.02508	0.84289	0.62052	0.14477
Heterotzxy (345)	0.93369	0.94747	0.84024	0.64972
ASD (167)	0.00002	0.98771	0.00001	0.04726
ToF (702)	0.87008	0.84625	0.67232	0.40356
Conotruncal (2569)	0.22075	0.19740	0.04527	0.46164

Test variants have MAF < 0.001 in gnomAD AND CADD > 20
Ultrarare variants do not appear in gnomAD
3740 previously published CHD probands

LVOTO: Left ventricular outflow tract obstruction; HLHS: Hypoplastic Left Heart Syndrome; ASD: Atrial Septal Defect; ToF: Tetralogy of Fallot
MAF: minor allele frequency
CADD: combined annotation-dependent depletion score

Table S2. Echocardiography of WT versus *Prrc2b*$^{p.R1128X/p.R1128X}$ KI (FL-*Prrc2b*^{gKO}) mice at the age of 1-3 months at baseline. Data is shown as mean ± SD. Technical replicates for each biological sample are plotted (WT: N=13; KI: N=14). An unpaired two-tailed Student t-test was performed to compare two groups for G. * $P < 0.05$; ** $P < 0.01$.

Month 1 (P30)	WT	KI (homozygous)
Heart Rate	550.23 ± 22.89	558.54 ± 33.64
Internal Diameter, Systole	1.74 ± 0.14	1.87 ± 0.32
Internal Diameter, Diastole	3.06 ± 0.14	3.15 ± 0.31
Volume;s	9.12 ± 2.00	11.33 ± 5.06
Volume;d	36.77 ± 4.22	40.04 ± 10.27
Stroke Volume	27.65 ± 3.44	28.71 ± 6.07
Ejection Fraction	75.25 ± 4.37	72.50 ± 6.70
Fractional Shortening	42.92 ± 3.76	40.84 ± 5.82
Cardiac Output	15.21 ± 1.99	15.98 ± 3.02
LV Mass	60.44 ± 8.34	58.16 ± 16.72
LV Mass Cor	48.35 ± 6.67	46.53 ± 13.38
LV Anterior Wall Diameter, Systole	0.94 ± 0.09	0.88 ± 0.17
LV Anterior Wall Diameter, Diastole	0.71 ± 0.05	0.65 ± 0.11
LV Posterior Wall Diameter, Systole	0.95 ± 0.11	0.87 ± 0.11
LV Posterior Wall Diameter, Diastole	0.64 ± 0.05	0.61 ± 0.07

Month 2 (P60)	WT	KI (homozygous)
Heart Rate	539.27 ± 24.08	595.31 ± 27.75
Internal Diameter, Systole	1.74 ± 0.26	1.81 ± 0.24
Internal Diameter, Diastole	3.16 ± 0.23	3.21 ± 0.22
Volume;s	9.28 ± 3.57	10.17 ± 3.18
Volume;d	39.98 ± 7.05	41.69 ± 6.99
Stroke Volume	30.70 ± 4.78	31.52 ± 5.31
Ejection Fraction	77.24 ± 6.00	75.83 ± 5.87
Fractional Shortening	45.08 ± 5.60	43.79 ± 5.48
Cardiac Output	16.56 ± 2.66	18.80 ± 3.49
LV Mass	61.55 ± 9.83	63.02 ± 10.75
LV Mass Cor	49.24 ± 7.86	50.42 ± 8.60
LV Anterior Wall Diameter, Systole	0.88 ± 0.09	0.95 ± 0.09
LV Anterior Wall Diameter, Diastole	0.67 ± 0.07	0.70 ± 0.07
LV Posterior Wall Diameter, Systole	0.97 ± 0.10	0.90 ± 0.12
LV Posterior Wall Diameter, Diastole	0.65 ± 0.06	0.62 ± 0.07

Month 3 (P90)	WT	KI (homozygous)
Heart Rate	556.20 ± 29.78	561.19 ± 30.88
Internal Diameter, Systole	2.06 ± 0.39	1.92 ± 0.28
Internal Diameter, Diastole	3.33 ± 0.29	3.33 ± 0.25
Volume;s	14.54 ± 6.47	11.97 ± 4.59
Volume;d	45.55 ± 9.62	45.55 ± 8.77
Stroke Volume	31.01 ± 5.46	33.57 ± 5.30
Ejection Fraction	69.17 ± 9.23	74.31 ± 6.02
Fractional Shortening	38.55 ± 7.95	42.48 ± 5.26
Cardiac Output	17.28 ± 3.39	18.78 ± 2.58
LV Mass	68.23 ± 16.05	69.13 ± 12.11
LV Mass Cor	54.58 ± 12.84	55.31 ± 9.69
LV Anterior Wall Diameter, Systole	0.88 ± 0.17	0.91 ± 0.15
LV Anterior Wall Diameter, Diastole	0.68 ± 0.10	0.70 ± 0.08
LV Posterior Wall Diameter, Systole	0.84 ± 0.16	0.91 ± 0.08
LV Posterior Wall Diameter, Diastole	0.65 ± 0.12	0.65 ± 0.06

Table S3. Differentially expressed genes in the whole hearts from the bulk RNA-seq of WT versus *Prrc2b*$^{tm1b-/-}$ mice at E18.5 (N=3 WT and N=2 *Prrc2b*$^{tm1b-/-}$ from the same litter).

Table S4. Differentially expressed genes in smooth muscle cells and cardiomyocytes from the single nucleus (sn)RNA-seq of WT versus *Prrc2b*$^{tm1b-/-}$ mice at E18.5 (N=3 WT and N=3 *Prrc2b*$^{tm1b-/-}$ combined).

Table S5. Differentially expressed proteins in whole hearts from the quantitative mass spectrometry analysis of WT versus *Prrc2b*$^{tm1b-/-}$ mice at E18.5 (N=3 WT and N=3 *Prrc2b*$^{tm1b-/-}$).

Table S6. List of primer sets

For genotyping:

Gene	Sequence (5' – 3')
mPrrc2b Tm1b 6tm-f (for tm1b)	Forward: GCACATGGCTGAATATCGACGGT
mPrrc2b Tm1b 7tm-r (for tm1b)	Reverse: ACTGATGGCGAGCTCAGACCATAAC
mPrrc2b WT-f (for WT)	Forward: AACTCACAGAGAGTGCCCAGA
mPrrc2b WT-r (for WT)	Reverse: CATAAGCTCTGATTCCCACAGA
hPRRC2B SEQ-F (for *Prrc2b*^{R1128X} KI)	Forward: AAAGGCAGATAAGACCTGGGAG
hPRRC2B SEQ-R (for *Prrc2b*^{R1128X} KI)	Reverse: GTTCTTTGGCAACAAAGGTTCT

For real-time PCR:

Primer	Sequence (5' – 3')
mPrrc2b Ex2,3-f	Forward: CCTCAGTTATTCCTAGACATGGC
mPrrc2b Ex2,3-r	Reverse: TGGGAACTATCA
mPrrc2b Ex3,5-f	Forward: GTGATAGTTCCCAAGGACGG
mPrrc2b Ex3,5-r	Reverse: CACCTTCGTGTCCGACTGGCT
human_exon15_F	Forward: AGGATCAGAACTGTGTGCCC
human_exon16_R	Reverse: GCTTGGGCCTTCTTGTCAAA
human_exon15+16_F	Forward: CATGCGTGTCAGGAATGAAAGC
human_exon16+17_F	Forward: GAAAGTGAAAAGATCCCCAGAC
human_exon15+17_F(1)	Forward: CATGCGTGTCAGATCCCCAGAC
human_exon15+17_F(2)	Forward: GCGTGTCAGATCCCCAGAC
human_exon17_R	Reverse: CTGTTTCATGGCCTCTCCCT
mPrrc2b Ex17,21-f	Forward: TGACCTGGGCTATGGAAATG
mPrrc2b Ex17,21-r	Reverse: CTCAAGTCAACGCCACTATCT
mPrrc2b Ex21,23-f	Forward: TAAGAGCAGCCAGGGAGATA
mPrrc2b Ex21,23-r	Reverse: GATTCCCTACAGGACCAGAAAC
mPrrc2b Ex24,25-f	Forward: CGCAGACCTCACACTAAAGATG
mPrrc2b Ex24,25-r	Reverse: AGCTGTAGTTGACCCCATTG
mPrrc2b Ex28,32-f	Forward: GCCCTGGTCTACGAGGGCC
mPrrc2b Ex28,32-r	Reverse: TCAGGCTTTGCTTCCCTCCACC
mouse_exon15_F	Forward: TCTACCCCTCAGCCCTGCAT
mouse_exon16_R	Reverse: AAGTCTGCTTGGGCCTTCTTGTC
mouse_exon15+16_F	Forward: GCATGCATGTCAGGAATGAAAG
mouse_exon16+17_F	Forward: GAAAGTCAAAAGGTCTCCAGATG
mouse_exon15+17_F	Forward: CATGCATGTCAGGTCTCCAGATG
mouse_exon17_R	Reverse: TCCATAGCCCAGGTCAAACT
Gapdh-f	Forward: CTTTGTCAAGCTCATTTCCTGG
Gapdh-r	Reverse: TCTTGCTCAGTGTCCTTGC
18srRNA-f	Forward: GCAATTATTCCCCATGAACG
18srRNA-r	Reverse: GGCCTCACTAAACCATCCAA
Myh11-f	Forward: AAGCTGCGGCTAGAGGTCA
Myh11-r	Reverse: CCCTCCCTTTGATGGCTGAG
Smarca4-f	Forward: CCATCCTGGAGCACGAGGAGC
Smarca4-r	Reverse: GGTCCATGCGCATGAACAGATC
Acta2-f	Forward: CCCCCTCTAGTGGTCAGGAA
Acta2-r	Reverse: ACGCTCTCAAATACCCCGTT
Actg2-f	Forward: CCGCCCTAGACATCAGGGT
Actg2-r	Reverse: TCTTCTGGTGCTACTCGAAGC
Bmp2-f	Forward: CGCAGCTTCCATCACGAA
Bmp2-r	Reverse: TGCAGATGTGAGAAACTCGTC
Hpgd-f	Forward: ATGTCTTCATTAGCAGGGCTC
Hpgd-r	Reverse: CATTCAGTCTTACACCGCTTTTC
Slco2a1-f	Forward: GTGAACCAGGATGAAAAGTCG

Slco2a1-r	Reverse: ATAAAGGGATGGAGATGGCAG
mt-Nd2-f	Forward: TTTACCCGCTACTCAACTCT
mt-Nd2-r	Reverse: TATTCATCCTATGTGGGCAAT
mt-Atp6-f	Forward: ATTATTGAAACAATTAGCCTA
mt-Atp6-r	Reverse: TTATTAATACTAGAGTAGCTCC

Acknowledgments

We thank Jiangbin Wu for his technical assistance and Tianlong Zhang for his help with structure prediction using AlphaFold web tool. We appreciate the technical assistance from Erika Flores Medina in histology and Amy Mohan, Deanne Mickelsen, and Christine Christie in surgical operations (Aab CVRI). We thank INFRAFRONTIER/EMMA for providing the mutant mouse line (C57BL/6N-A<tm1Brd>*Prrc2b*<tm1a(EUCOMM)Wtsi>/WtsiBiat (frozen sperms)), INFRAFRONTIER/EMMA (www.infrafrontier.eu, PMID: 25414328), from which the mouse line was distributed (EM:05981). Associated primary phenotypic information may be found at www.mousephenotype.org. We also appreciate the technical assistance from Lin Gan for *in vitro* fertilization and generating the *Prrc2b* tm1a mouse line on a service fee basis. We acknowledge the Pediatric Cardiac Genetics Consortium (PCGC) for providing the published data of genetic variants within the PRRC2B gene of 3,740 CHD probands in the PCGC genetic mutation databases.

Author contributions

PY launched the study and obtained the funding. PY, DD, ESK, and FJ conceived the ideas, designed the experiments, analyzed the data, and wrote the manuscript. DD, ESK, FJ, JH, YK, HL, and FM conducted the experimental work. FJ and JG performed the bioinformatic analysis. JG, ZJ, PM, and GAP provided technical assistance, conceptual feedback, or contributed to experimental work. All the authors discussed the results and had the opportunity to comment on the manuscript.

Competing interests

None of the authors declares any competing interests.

SOURCES OF FUNDING

This work was supported by National Institutes of Health grants R01 HL132899, R01 HL147954, R01 HL164584, R01 HL169432, 24EIA1255341, and the Harold S. Geneen Charitable Trust Awards Program for Coronary Heart Disease Research (to P.Y.), R01 HL144776 (to GAP), and R01 HL141171 and R01 HL130167 (to Z.J.).

Reference

1. Gao, C. and Wang, Y. (2020) mRNA Metabolism in Cardiac Development and Disease: Life After Transcription. *Physiol Rev*, **100**, 673-694.
2. Kalsotra, A. and Cooper, T.A. (2011) Functional consequences of developmentally regulated alternative splicing. *Nat Rev Genet*, **12**, 715-729.
3. Tahmasebi, S., Khoutorsky, A., Mathews, M.B. and Sonenberg, N. (2018) Translation deregulation in human disease. *Nat Rev Mol Cell Biol*, **19**, 791-807.
4. Castello, A., Fischer, B., Eichelbaum, K., Horos, R., Beckmann, B.M., Strein, C., Davey, N.E., Humphreys, D.T., Preiss, T., Steinmetz, L.M. *et al.* (2012) Insights into RNA biology from an atlas of mammalian mRNA-binding proteins. *Cell*, **149**, 1393-1406.
5. Baltz, A.G., Munschauer, M., Schwanhausser, B., Vasile, A., Murakawa, Y., Schueler, M., Youngs, N., Penfold-Brown, D., Drew, K., Milek, M. *et al.* (2012) The mRNA-bound proteome and its global occupancy profile on protein-coding transcripts. *Mol Cell*, **46**, 674-690.
6. Castello, A., Fischer, B., Frese, C.K., Horos, R., Alleaume, A.M., Foehr, S., Curk, T., Krijgsveld, J. and Hentze, M.W. (2016) Comprehensive Identification of RNA-Binding Domains in Human Cells. *Mol Cell*, **63**, 696-710.
7. Sugiyama, H., Takahashi, K., Yamamoto, T., Iwasaki, M., Narita, M., Nakamura, M., Rand, T.A., Nakagawa, M., Watanabe, A. and Yamanaka, S. (2017) Nat1 promotes translation of specific proteins that induce differentiation of mouse embryonic stem cells. *Proc Natl Acad Sci U S A*, **114**, 340-345.
8. Jiang, F., Hedaya, O.M., Khor, E., Wu, J., Auguste, M. and Yao, P. (2023) RNA binding protein PRRC2B mediates translation of specific mRNAs and regulates cell cycle progression. *Nucleic Acids Res*.
9. Mei, Q., Liu, J., Liu, Y., Li, C., Wang, H., Li, H., Chen, X. and Lan, X. (2013) Expression of proline-rich coiled-coil 2B protein in developing rat brains. *Neurosci Lett*, **557 Pt B**, 171-176.
10. Li, S., Hu, W., Gong, S., Zhang, P., Cheng, J., Wang, S., Wang, Y., Shi, W., Li, Q., Wang, F. *et al.* (2023) The Role of PRRC2B in Cerebral Vascular Remodeling Under Acute Hypoxia in Mice. *Adv Sci (Weinh)*, **10**, e2300892.
11. Sevim Bayrak, C., Zhang, P., Tristani-Firouzi, M., Gelb, B.D. and Itan, Y. (2020) De novo variants in exomes of congenital heart disease patients identify risk genes and pathways. *Genome Med*, **12**, 9.
12. Jin, S.C., Homsy, J., Zaidi, S., Lu, Q., Morton, S., DePalma, S.R., Zeng, X., Qi, H., Chang, W., Sierant, M.C. *et al.* (2017) Contribution of rare inherited and de novo variants in 2,871 congenital heart disease probands. *Nat Genet*, **49**, 1593-1601.
13. Russell, I.A., Rouine-Rapp, K., Stratmann, G. and Miller-Hance, W.C. (2006) Congenital heart disease in the adult: a review with internet-accessible transesophageal echocardiographic images. *Anesth Analg*, **102**, 694-723.
14. Bohlen, J., Roiuk, M., Neff, M. and Teleman, A.A. (2023) PRRC2 proteins impact translation initiation by promoting leaky scanning. *Nucleic Acids Res*.

15. Jumper, J., Evans, R., Pritzel, A., Green, T., Figurnov, M., Ronneberger, O., Tunyasuvunakool, K., Bates, R., Zidek, A., Potapenko, A. *et al.* (2021) Highly accurate protein structure prediction with AlphaFold. *Nature*, **596**, 583-589.
16. Varadi, M., Anyango, S., Deshpande, M., Nair, S., Natassia, C., Yordanova, G., Yuan, D., Stroe, O., Wood, G., Laydon, A. *et al.* (2022) AlphaFold Protein Structure Database: massively expanding the structural coverage of protein-sequence space with high-accuracy models. *Nucleic Acids Res*, **50**, D439-D444.
17. Wang, Y.J., Zhang, X., Lam, C.K., Guo, H., Wang, C., Zhang, S., Wu, J.C., Snyder, M. and Li, J. (2022) Systems analysis of de novo mutations in congenital heart diseases identified a protein network in the hypoplastic left heart syndrome. *Cell Syst*, **13**, 895-910 e894.
18. Morton, S.U., Shimamura, A., Newburger, P.E., Opotowsky, A.R., Quiat, D., Pereira, A.C., Jin, S.C., Gurvitz, M., Brueckner, M., Chung, W.K. *et al.* (2021) Association of Damaging Variants in Genes With Increased Cancer Risk Among Patients With Congenital Heart Disease. *JAMA Cardiol*, **6**, 457-462.
19. Castello, A., Fischer, B., Frese, Christian K., Horos, R., Alleaume, A.-M., Foehr, S., Curk, T., Krijgsveld, J. and Hentze, Matthias W. (2016) Comprehensive Identification of RNA-Binding Domains in Human Cells. *Molecular Cell*, **63**, 696-710.
20. Schneider, A., Guan, Y., Zhang, Y., Magnuson, M.A., Pettepher, C., Loftin, C.D., Langenbach, R., Breyer, R.M. and Breyer, M.D. (2004) Generation of a conditional allele of the mouse prostaglandin EP4 receptor. *Genesis*, **40**, 7-14.
21. Baeten, J.T., Jackson, A.R., McHugh, K.M. and Lilly, B. (2015) Loss of Notch2 and Notch3 in vascular smooth muscle causes patent ductus arteriosus. *Genesis*, **53**, 738-748.
22. Lewis, T.R., Shelton, E.L., Van Driest, S.L., Kannankeril, P.J. and Reese, J. (2018) Genetics of the patent ductus arteriosus (PDA) and pharmacogenetics of PDA treatment. *Semin Fetal Neonatal Med*, **23**, 232-238.
23. Hosur, V., Low, B.E., Li, D., Stafford, G.A., Kohar, V., Shultz, L.D. and Wiles, M.V. (2020) Genes adapt to outsmart gene-targeting strategies in mutant mouse strains by skipping exons to reinitiate transcription and translation. *Genome Biol*, **21**, 168.
24. Crockett, S.L., Berger, C.D., Shelton, E.L. and Reese, J. (2019) Molecular and mechanical factors contributing to ductus arteriosus patency and closure. *Congenit Heart Dis*, **14**, 15-20.
25. Satoda, M., Pierpont, M.E.M., Diaz, G.A., Bornemeier, R.A. and Gelb, B.D. (1999) Char syndrome, an inherited disorder with patent ductus arteriosus, maps to chromosome 6p12-p21. *Circulation*, **99**, 3036-3042.
26. Zhang, M., Chen, M., Kim, J.R., Zhou, J.L., Jones, R.E., Tune, J.D., Kassab, G.S., Metzger, D., Ahlfeld, S., Conway, S.J. *et al.* (2011) SWI/SNF Complexes Containing Brahma or Brahma-Related Gene 1 Play Distinct Roles in Smooth Muscle Development. *Molecular and Cellular Biology*, **31**, 2618-2631.
27. Morano. (2000) Smooth-muscle contraction without smooth-muscle myosin (vol 2, pg 371, 2000). *Nature Cell Biology*, **2**, 676-676.
28. Pen, A., Moreno, M.J., Durocher, Y., Deb-Rinker, P. and Stanimirovic, D.B. (2008) Glioblastoma-secreted factors induce IGFBP7 and angiogenesis by modulating Smad-2-dependent TGF-beta signaling. *Oncogene*, **27**, 6834-6844.

29. Homsy, J., Zaidi, S., Shen, Y., Ware, J.S., Samocha, K.E., Karczewski, K.J., DePalma, S.R., McKean, D., Wakimoto, H., Gorham, J. *et al.* (2015) De novo mutations in congenital heart disease with neurodevelopmental and other congenital anomalies. *Science*, **350**, 1262-1266.
30. Zaidi, S., Choi, M., Wakimoto, H., Ma, L., Jiang, J., Overton, J.D., Romano-Adesman, A., Bjornson, R.D., Breitbart, R.E., Brown, K.K. *et al.* (2013) De novo mutations in histone-modifying genes in congenital heart disease. *Nature*, **498**, 220-223.
31. Van der Auwera, G.A., Carneiro, M.O., Hartl, C., Poplin, R., Del Angel, G., Levy-Moonshine, A., Jordan, T., Shakir, K., Roazen, D., Thibault, J. *et al.* (2013) From FastQ data to high confidence variant calls: the Genome Analysis Toolkit best practices pipeline. *Curr Protoc Bioinformatics*, **43**, 11 10 11-11 10 33.
32. McKenna, A., Hanna, M., Banks, E., Sivachenko, A., Cibulskis, K., Kernytsky, A., Garimella, K., Altshuler, D., Gabriel, S., Daly, M. *et al.* (2010) The Genome Analysis Toolkit: a MapReduce framework for analyzing next-generation DNA sequencing data. *Genome Res*, **20**, 1297-1303.
33. Purcell, S., Neale, B., Todd-Brown, K., Thomas, L., Ferreira, M.A., Bender, D., Maller, J., Sklar, P., de Bakker, P.I., Daly, M.J. *et al.* (2007) PLINK: a tool set for whole-genome association and population-based linkage analyses. *Am J Hum Genet*, **81**, 559-575.
34. Navarro Gonzalez, J., Zweig, A.S., Speir, M.L., Schmelter, D., Rosenbloom, K.R., Raney, B.J., Powell, C.C., Nassar, L.R., Maulding, N.D., Lee, C.M. *et al.* (2021) The UCSC Genome Browser database: 2021 update. *Nucleic Acids Res*, **49**, D1046-D1057.
35. Wang, K., Li, M. and Hakonarson, H. (2010) ANNOVAR: functional annotation of genetic variants from high-throughput sequencing data. *Nucleic Acids Res*, **38**, e164.
36. Kircher, M., Witten, D.M., Jain, P., O'Roak, B.J., Cooper, G.M. and Shendure, J. (2014) A general framework for estimating the relative pathogenicity of human genetic variants. *Nat Genet*, **46**, 310-315.
37. Karczewski, K.J., Francioli, L.C., Tiao, G., Cummings, B.B., Alfoldi, J., Wang, Q., Collins, R.L., Laricchia, K.M., Ganna, A., Birnbaum, D.P. *et al.* (2020) The mutational constraint spectrum quantified from variation in 141,456 humans. *Nature*, **581**, 434-443.
38. Wu, M.C., Lee, S., Cai, T., Li, Y., Boehnke, M. and Lin, X. (2011) Rare-variant association testing for sequencing data with the sequence kernel association test. *Am J Hum Genet*, **89**, 82-93.
39. Bolger, A.M., Lohse, M. and Usadel, B. (2014) Trimmomatic: a flexible trimmer for Illumina sequence data. *Bioinformatics*, **30**, 2114-2120.
40. Kim, D., Paggi, J.M., Park, C., Bennett, C. and Salzberg, S.L. (2019) Graph-based genome alignment and genotyping with HISAT2 and HISAT-genotype. *Nat Biotechnol*, **37**, 907-915.
41. Liao, Y., Smyth, G.K. and Shi, W. (2014) featureCounts: an efficient general purpose program for assigning sequence reads to genomic features. *Bioinformatics*, **30**, 923-930.
42. Frankish, A., Diekhans, M., Jungreis, I., Lagarde, J., Loveland, J.E., Mudge, J.M., Sisu, C., Wright, J.C., Armstrong, J., Barnes, I. *et al.* (2021) GENCODE 2021. *Nucleic Acids Res*, **49**, D916-d923.
43. Love, M.I., Huber, W. and Anders, S. (2014) Moderated estimation of fold change and dispersion for RNA-seq data with DESeq2. *Genome Biology*, **15**, 550.

44. Team, R.C.R. (2020) A language and environment for statistical computing. R Foundation for Statistical Computing, Vienna, Austria. . *Vienna, Austria. URL https://www.R-project.org/. (2020).*
45. Wu, T., Hu, E., Xu, S., Chen, M., Guo, P., Dai, Z., Feng, T., Zhou, L., Tang, W., Zhan, L. *et al.* (2021) clusterProfiler 4.0: A universal enrichment tool for interpreting omics data. *Innovation (Camb)*, **2**, 100141.